Nearby Galaxies in the 2μm All Sky Survey I. K-band Luminosity Functions

Nick Devereux[1]

Department of Physics, Embry-Riddle Aeronautical University, Prescott, AZ 86301

devereux@erau.edu

S.P. Willner & M.L.N. Ashby

Harvard-Smithsonian Center for Astrophysics

swillner@cfa.harvard.edu, mashby@cfa.harvard.edu

C.N.A. Willmer

University of Arizona

cnaw@as.arizona.edu

and

Paul Hriljac

Department of Mathematics and Computer Science, Embry-Riddle Aeronautical University, Prescott, AZ 86301

hriljap@erau.edu

ABSTRACT

Differential K_s-band luminosity functions (LFs) are presented for a complete sample of 1613 nearby bright galaxies segregated by visible morphology. The LF for late-type spirals follows a power law that rises towards low luminosities whereas the LFs for ellipticals, lenticulars and bulge-dominated spirals are peaked and decline toward both higher and lower luminosities. Each morphological type (E, S0, S0/a–Sab, Sb–Sbc, Sc–Scd) contributes approximately equally to the overall K_s-band luminosity density of galaxies in the local universe. Type

[1]Fulbright Scholar, Center for Astronomy, National University of Ireland, Galway

averaged bulge/disk ratios are used to subtract the disk component leading to the prediction that the K_s-band LF for bulges is bimodal with ellipticals dominating the high luminosity peak, comprising 60% of the bulge luminosity density in the local universe with the remaining 40% contributed by lenticulars and the bulges of spirals. Overall, bulges contribute 30% of the galaxy luminosity density at K_s in the local universe with spiral disks making up the remainder. If bulge luminosities indicate central black hole masses, then our results predict that the black hole mass function is also bimodal.

Subject headings: galaxies: luminosity function, mass function — galaxies: formation — galaxies: elliptical and lenticular, cD — galaxies: spiral — galaxies: bulges — infrared: galaxies

1. Introduction

Luminosity functions (LFs) are one of the key statistical instruments widely used to better our understanding of galaxies, because with just a few parameters, they concisely describe entire populations of objects whose intrinsic properties (e.g., mass, luminosity, etc.) vary over orders of magnitude. In the Schechter (1976) formulation, those parameters are M^*, the absolute magnitude corresponding to the knee of the LF, ϕ^*, the mean galaxy space density, and α, the faint-end slope of the LF. The basic technique is to measure and then compare these parameters for different populations and thereby assess, for example, how galaxies evolve with redshift, or as a function of environment, or indeed any other variable that can be controlled for. This tool has been used, as of late, to analyse several large samples of galaxies reaching out to redshifts $z \sim 1$ and beyond (e.g., Norberg et al. 2002; Blanton et al. 2003; Wolf et al. 2003; Bell et al. 2003; Ilbert et al. 2005; Willmer et al. 2006; Brown et al. 2007; Faber et al. 2007; Wake et al. 2006; Reddy et al. 2008).

Galaxy morphology is a taxonomy devised by Hubble (1936) and refined by de Vaucouleurs (1959) and de Vaucouleurs et al. (1991) that is based on the relative prominence of the stellar bulge and the degree of resolution of the spiral arms. The physical significance of galaxy morphology is that it reflects the galaxy merger history (e.g., Balland, Silk, & Schaeffer 1998). It is conventional wisdom that the galaxy LF does depend on morphology in the B-band. Sandage, Binggeli & Tammann (1985) found that LFs depend on morphological type for galaxies in the Virgo cluster and subsequent works showed that this dependence extends to field galaxies (Binggeli, Sandage & Tammann 1988; Loveday et al. 1992). However, Efstathiou, Ellis, & Peterson (1988) and Marzke et al. (1994, 1998) offer a contrary

view. More recently, LFs based on morphological proxies[1], such as color, also show a dependence (e.g., Blanton et al. 2001; Bell et al. 2004; Blanton 2006; Willmer et al. 2006; Faber et al. 2007), at least at visible wavelengths. These studies and others indicate that the present-day LFs are the result of a complex evolutionary history.

By virtue of its uniformity, reliability, and full-sky coverage, the Two Micron All Sky Survey (2MASS, Skrutskie et al. 2006) has recently made it possible to extend LF studies into the infrared regime. 2MASS has been exploited in recent years to produce near-infrared luminosity functions for galaxies with ever greater precision, facilitated by redshifts generated from the SDSS (York et al. 2000) and the 2 and 6 degree Field Galaxy Redshift Surveys (Cole et al. 2001; Kochanek et al. 2001; Bell et al. 2003; Eke et al. 2005; Jones et al. 2006). The 2.16μm K_s-band (hereafter K-band) LF is of particular interest because of its relevance to understanding galaxy evolution in the context of Lambda Cold Dark Matter (ΛCDM) cosmology: at $z = 0$, the K-band light traces the stellar mass accumulated in galaxies at a wavelength where interstellar extinction is minimal (Devereux, Becklin & Scoville 1987; Bell & de Jong 2001; Bell et al. 2003), avoiding strong dependence on metallicity and stellar population age. For this reason, K-band LFs complement those obtained at visible wavelengths.

Both Kochanek et al. (2001) and Bell et al. (2003) investigated the impact of morphology on the K-band LF. Bell et al. (2003) used an SDSS concentration parameter (c_r) as a proxy for type. Kochanek et al. (2001) carried out a painstaking typing procedure in such a way as to permit a quantitative understanding of the uncertainties involved. Both studies divided the galaxy samples into two broad categories; early and late. They arrived at consistent total K-band LFs (Bell et al. 2003, Figure 9), and found that the early- and late-type LFs were well-described by Schechter functions that differed slightly in M^* and ϕ^*, but had essentially identical shapes. This is somewhat surprising given the distinctions revealed by LFs measured in the visible. Clearly more work remains to be done on the morphological type dependence of LFs in general, and for the K-band LF in particular. Fortunately, the time-consuming task of assigning visible morphologies has now been completed for the vast majority of nearby galaxies. The principal aim of this paper is therefore to use these nearby galaxies to define new benchmark K-band LFs for galaxies. As such, our study offers an improvement on Kochanek et al. (2001) and Bell et al. (2003) by using the most recent distances and *finely divided* morphological types.

[1]Morphological proxies such as color are adopted until the difficult and time consuming task of assigning morphologies to the ever-growing number of cataloged galaxies can be accomplished e.g.,The Galaxy Zoo Project, http://www.galaxyzoo.org/

The paper is organized as follows. Section 2 describes how the nearby galaxy sample is selected. A non-parametric (Choloniewski) method is used to generate the LFs as described in section 3. The results, presented in section 4, include the morphological type dependence of the K-band LFs as well as the contribution of each to the luminosity density in the local universe. Recently published data have also provided the opportunity to compute the bulge luminosity functions and hence the contribution of bulges and disks to the K-band luminosity density in the local universe. These results are also presented in section 4. A discussion, in section 5, explains how the results may be used to constrain models of galaxy evolution and includes a prediction that the bulge LF and by association, the black hole mass function, is bimodal and depends on Hubble type. Conclusions follow in Section 6.

2. Sample Selection

The goal of this study is to quantify the dependence of the K-band LFs on the visual appearance of galaxies. This dictates that the sample be composed of nearby galaxies which have the most reliable morphological assignments. Nearby galaxies were identified using HYPERLEDA; a web-based interface (http://leda.univ-lyon1.fr) that provides access to the Principal Galaxy Catalog (hereafter PGC, Paturel et al. 2003). The PGC is a homogeneous database of galaxy parameters in the sense that an attempt has been made to place independent measures on a standard system. Parameters employed in this study include coordinates accurate to $\sim 2''$, visible morphological `T` types and recession velocities for all known galaxies brighter than $B = 18\,\mathrm{mag}$. The PGC is a dynamic resource that is constantly being updated, but as of 2008 January there were 7406 nearby galaxies with $\mathrm{V}_{gsr} \leq 3000\,\mathrm{km\,s^{-1}}$, apparent total blue magnitudes $\mathrm{m}_B \leq 18\,\mathrm{mag}$ and Galactic latitudes $|b| > 10$ degrees. The latitude constraint was imposed to avoid the inevitable incompleteness due to obscuration within our galaxy. However, with the exception of the Galactic plane, the PGC galaxies from which the sample is selected are distributed over the entire sky thereby minimizing the effect of cosmic variance due to large scale structures present in the sample volume.

The 2MASS counterparts of the PGC galaxies were identified on the basis of positional coincidence. For an association to be made, the PGC J2000 coordinate had to fall within $10''$ of the 2MASS J2000 coordinate listed in the Extended Source Catalog[2](XSC, Jarrett et al. 2000). This comparison yielded 5034 detections at $2.2\,\mu$m (K-band) corresponding to a 68%

[2]Final checking revealed 30 galaxies with PGC and XSC coordinate differences greater than $10''$. The discrepancy is due to different centroids in visible and infrared light which is a problem particularly for nearby galaxies of large angular size. These galaxies are included in Table 1.

detection rate. Figure 1 shows the distribution of apparent K-band isophotal magnitudes for nearby galaxies ($V_{gsr} \leq 3000\,km\,s^{-1}$) in the 2MASS XSC. The distribution turns over at $K = 10$ mag indicating that the XSC is incomplete for galaxies fainter than that. On this basis, a volume-limited sample was defined for further study, hereafter the K10/3000 sample, comprising 1613 galaxies with $K \leq 10$ mag, $V_{gsr} \leq 3000\,km\,s^{-1}$, and $|b| > 10$ degrees (Table 1). The choice to use V_{gsr} allows us to define a spherical volume centered on the Milky Way that simplifies the LF calculation.

Every attempt has been made to identify all known galaxies with $K \leq 10$ mag, $V_{gsr} \leq 3000\,km\,s^{-1}$, and $|b| > 10$ degrees. Nevertheless, sample incompleteness can arise in two ways: 1) galaxies that are in the 2MASS XSC but have no radial velocities in the PGC or are missing from the PGC altogether, and 2) PGC galaxies missing from the XSC. A firm upper limit on the former can be set by noting that there are 388 objects with $K \leq 10$ and $|b| > 10$ degrees in the 2MASS XSC for which no association with a PGC galaxy can be found. Inspection of 2MASS images reveals that most are Galactic star clusters (or indeed in some cases small parts of star clusters treated by the automated XSC extraction procedure as distinct objects), but some are galaxies. Redshifts have been determined by J. Huchra, L. Macri, T. Jarrett, J. Mader, A. Crook, R. Cutri, T. George, N. Martimbeau, S. Schneider, & M. Skrutskie (ApJ Supp., 2009, in preparation) for all 166 of the galaxies. All but three of which have radial velocities $>3000\,km\,s^{-1}$. The three with $V < 3000$ km s^{-1} should in principle be included in the K10/3000 sample but are not because they have no entries in the PGC; this gives an estimated completeness for Table 1 of 99.8%. With regard to the second source of incompleteness, there are two well known PGC galaxies of large angular size missing from the 2MASS XSC: the Large and Small Magellanic Clouds. These and some other local group dwarf galaxies are not included in the XSC (Jarrett et al. 2003) and hence are not included in the K10/3000 sample. However, it is unlikely that there are any PGC spiral and elliptical galaxies missing from the K10/3000 sample because the $K = 10$ sample limit corresponds to $B = 13.5$ for a normal $B - K = 3.5$ galaxy color, which is 4.5 magnitudes brighter than the PGC catalog limit. Thus, only galaxies with very blue colors and/or very low surface brightness would be missing from our sample (Andreon 2002) and both selection effects will tend to further bias our sample against late-type (Sd and later) spirals and dwarf irregular (Im) galaxies, as explained in more detail in the next section.

2.1. Morphological Types in the K10/3000 Sample

The observed distribution of K magnitudes for galaxies in the XSC with $V_{gsr} \leq 3000\,km\,s^{-1}$ is compared with the distribution of blue magnitudes for the entire inventory of 7406 PGC

galaxies contained within the same volume (Figure 1). The figure shows that 2MASS detected essentially the same number of nearby galaxies with $K \leq 10$ mag as would be found in a B-band selected sample with $B \leq 13.5$ mag.

Figure 2 illustrates how the $B-K$ color distribution for a K-band limited sample differs from a B-band selected one. Although a B-band selected sample with $B \leq 13.5$ mag contains about as many galaxies as a K-band selected sample with $K \leq 10$ mag, the latter sample excludes blue galaxies contained between the two magnitude limits, figuratively speaking, between 6 and 8 o'clock on the plot. However, the deficiency is almost exactly compensated for by the inclusion of additional red galaxies between 12 and 2 o'clock. Thus, a K-band magnitude limited sample will contain more red and fewer blue galaxies compared to a B-band selected sample of similar size.

Since a K-band selected sample contains fewer blue galaxies compared to a B-band selected sample of comparable size, one can therefore anticipate that morphological types in the K10/3000 sample will contain fewer star forming late-type spirals and dwarf irregular galaxies, compared to a B-band selected sample of similar size. Figure 3 supports this expectation. The distribution of morphological types in the K10/3000 sample spans the entire range from ellipticals to dwarf irregulars. However, compared to the sample of PGC galaxies with $B \leq 13.5$ mag, the K10/3000 sample appears to be missing more than 50% of galaxies with morphological types T > 6, corresponding to Sd and later. Consequently, these types of galaxies will not be considered further as there are too few to reliably define a LF. On the other hand, the K-band is sensitive to the red luminous mass component in all galaxy types with the result that the K10/3000 sample contains 80% of the Sc–Scd types and all the earlier types, plus more, than would be found in a B-band selected sample of comparable size.

A completeness test that makes no assumptions concerning the galaxy distribution and is unaffected by the presence of large scale structure was proposed by Rauzy (2001). The test assumes that the LF of the population does not depend on the three-dimensional redshift-spatial distribution and that the apparent magnitude limit can be described by a sharp cutoff. In practice the test examines the distribution of the random variable

$$\zeta = \frac{\int_{-\infty}^{M} \phi(M) dM}{\int_{-\infty}^{M_{lim}(z)} \phi(M) dM} \tag{1}$$

which measures the ratio between the integrated LF up to the absolute magnitude of a given galaxy and the total range in magnitudes accessible at the distance of the galaxy.

Completeness is measured by the variable

$$T_c = \frac{\sum_{i=1}^{N_{gal}} (\zeta_i - 0.5)}{(\sum_{i=1}^{N_{gal}} V_i)^{1/2}} \tag{2}$$

where the V_i represent the variance of the ζ_i estimators. The T_c variable has an expectation value of zero and unit variance. In practice the test is evaluated for sub-samples selected at progressively fainter apparent magnitude limits. The T_c statistic will fluctuate around the value of zero, but becomes systematically negative once the sample becomes incomplete. From the behavior of this statistic the limiting magnitude can be inferred. Figure 4 illustrates the result of applying this test to the full K10/3000 sample and to several sub-samples segregated by morphological type. Both the number counts and the Rauzy tests suggest that the current sample is not affected by incompleteness for the morphological types we are considering, namely ellipticals, lenticulars and spirals up to and including types Scd.

2.2. Galaxy Distances

Because the sample galaxies are nearby, their peculiar velocities can be a significant fraction of their Hubble flow velocities, particularly for those with $V_{gsr} \leq 1000\,km\,s^{-1}$. Major perturbers include the Virgo cluster, which lies inside the sample volume, and the Great Attractor (Lynden-Bell et al. 1988) which lies outside the volume but still perturbs the Hubble flow within. Thus, one can not simply deduce a distance from the recession velocity and a Hubble constant. Tully et al. (2008) have recently quantified the peculiar velocities for nearby galaxies utilizing redshift-independent distances based on the following methods; the Tully-Fisher relation (Tully & Fisher 1977), Cepheids (Freedman et al. 2001), the luminosity of stars at the tip of the red giant branch (Karachentsev et al. 2004, 2006), and surface brightness fluctuations (Tonry et al. 2001). These methods have yielded *quality* distances, with distance modulus uncertainties < 0.1 mag, for 591 nearby ($V_{gsr} \leq 3000\,km\,s^{-1}$) galaxies of which 302 are included in the K10/3000 sample. Tully determined distances for other galaxies based on associations with groups which contain one or more members with quality distances together with the Numerical Action Models of Shaya et al. (1995). Collectively, datasets provided by Tully (2007, private communication) yielded distances for 1575 or 98% of the 1613 objects in the K10/3000 sample and they are listed in Table 1[3].

[3]See also The Extragalactic Distance Database (EDD) at http://edd.ifa.hawaii.edu/

2.3. 2MASS magnitudes

In the following analysis, isophotal magnitudes (measured within the 20 mag arcsec^{-2} elliptical isophote; the parameter: `k_m_k20fe` in the 2MASS XSC) are adopted to characterize the dependence of K-band LFs on galaxy morphology (section 4.2). The main reason for this choice is that the extrapolated total magnitudes published in the 2MASS XSC are unreliable for elliptical galaxies due to a restriction on the choice of Sérsic index that caused their total flux to be underestimated (Lauer et al. 2007), by an amount we determine to be $\sim$0.3 mag[4]. Additionally, extrapolated total magnitudes in the 2MASS XSC can lead to unphysical colors (Karachentsev et al. 2002) suggesting that the extrapolations are unreliable for some spiral galaxies as well. With the exception of the ellipticals, the mean difference between the isophotal and total magnitudes cited in the 2MASS XSC is small: about 0.14 mag for the bright, $K \leq 10$ mag, galaxies in our sample and is independent of galaxy type for morphologies spanning S0 to Scd. Thus, the isophotal magnitudes are adopted as published with no corrections with the understanding that they slightly underestimate the total magnitudes for spiral and lenticular galaxies but significantly underestimate the total magnitudes for ellipticals: a detail that is addressed in sections 4.3 and 4.4.

3. Luminosity Function Determination

The LF calculation uses the maximum likelihood method of Choloniewski (1986) which assumes that the spatial distribution of galaxies and their luminosities are uncorrelated. The merit of this common Poisson assumption is discussed further in the Appendix. By counting galaxies in a plane defined by distance and luminosity it is possible to obtain, simultaneously, the density distribution as a function of distance and the properly normalised LF, unaffected by density variations within the sample (Choloniewski 1986; Takeuchi, Yoshikawa & Ishii 2000). The Choloniewski method is non-parametric, i.e., it makes no assumptions of a functional form for the LF and it yields the overall normalization (galaxy space density) directly. A disadvantage is that it requires binning the data. These characteristics distinguish it from the maximum likelihood methods of Sandage, Tammann & Yahil (1979) and Efstathiou, Ellis, & Peterson (1988). The interested reader is referred to Willmer (1997) and Takeuchi, Yoshikawa & Ishii (2000) for a more detailed inter-comparison of the

[4]The average difference between the isophotal and total magnitudes quoted in the XSC is ~ 0.1 mag for K10/3000 elliptical galaxies. However, based on an analysis described in section 4.4, we find that the total magnitude is likely to be 0.3 mag brighter, on average, than the total magnitude quoted in the XSC for K10/3000 elliptical galaxies.

methods used to calculate galaxy LFs. Generally speaking, the results obtained using the Choloniewski method always agree, within the estimated statistical uncertainties, with the other methods described by Binggeli, Sandage & Tammann (1988); Willmer (1997) and Takeuchi, Yoshikawa & Ishii (2000). The same is true for the K10/3000 sample considered here.

The Choloniewski method is implemented by plotting the two independent quantities; distance modulus and absolute magnitude, as illustrated in Figure 5. Galaxies are then binned and summed, vertically and horizontally. A small penalty is incurred as a result of the binning procedure because galaxies contained in partial bins, that are bisected by the apparent magnitude limit of the survey, must be excluded. Additionally, a few galaxies are excluded by the upper and lower bounds of the absolute magnitude and distance modulus limits. Table 2 provides a summary of the binning parameters used to generate the various LFs presented in this paper. The summations are used to iteratively solve the simultaneous equations 18, 19, and 20 (or 21) cited by Choloniewski (1986). These non-linear equations converge surprisingly quickly to yield ϕ(M), the differential LF, where M is absolute magnitude, $\rho(\mu)$, the number density of galaxies as a function of distance modulus, μ, and n, the average number density of galaxies in the sample. The procedure was applied to the full K10/3000 sample and also to subsets of galaxies sorted by morphological type. A detailed explanation of how to correctly populate the covariance matrix, from which the statistical uncertainties are derived, is provided in the Appendix.

In order to test the LF calculation, it was applied to samples of size comparable to the K10/3000 sample drawn from the Millenium Simulation database (Springel et al. 2005) and in particular the semi-analytic galaxy catalog within it (De Lucia & Blaizot 2007; Croton et al. 2006). For 16 independent samples drawn according to the μ and m_K selection of the K10/3000 sample, the derived LFs agree well with the true one derived by counting all simulated galaxies within the volume. The dispersion among the 16 realizations is, however, about 50% larger than the calculated LF uncertainties, even after normalizing the 16 samples to eliminate cosmic variance. The excess dispersion is also about 50% larger than the Poisson uncertainties. Thus, to the extent that the Millenium Simulation is representative of the distribution of galaxies in the local universe, neither the Poisson estimate nor the Choloniewski estimate is a good representation of the actual uncertainties as measured by the standard deviation of the simulated LFs. The most likely reason for the discrepancy is that real galaxies are clustered. Clustering will increase the uncertainties because the statistically-independent unit consists of multiple galaxies (on average 2.2 of them if the uncertainties are increased by a factor of 1.5). The effect of clustering is discussed in more detail in the Appendix. For the Choloniewski method in particular, the discrepancy between the calculated uncertainties and their Poisson values is largest for elliptical, lenticular, and

early-type spirals (Table 3) which tend to be the most clustered. The Choloniewski uncertainty estimates thus seem particularly sensitive to clustering, but future improvements may be possible by implementing the method with a generalized Poisson distribution instead. Overall, the simulation results suggest that the LFs are reliable but the calculated uncertainties are underestimated by about a factor of 1.5 and using the Poisson method to estimate uncertainties would not improve the results.

4. Results

4.1. Density Function for the K10/3000 Sample

Figure 6 illustrates the solid-angle averaged radial number density of galaxies at each distance in the sample volume. Since the solid angle average is over very nearly the whole sky (3.3π steradians) individual structures can account for only a small fraction of any density peak. For example, the Virgo cluster, which is the largest structure in this volume, constitutes only $\sim 14\%$ of the total galaxy density enhancement seen at $\mu + 5\log_{10}h \sim 30.5$ mag. That peak is likely due to the combination of the Local Supercluster (of which Virgo is part) and the Southern Supercluster (a Southern hemisphere structure that includes the groups of Dorado and the Eridanus and Fornax clusters). Consequently, one is cautioned against identifying density enhancements with individual known galaxy clusters or groups. Clear evidence for a morphology-density relation (Dressler 1980) is therefore absent from the data. Late-type spirals (Sc–Scd) have the highest average number density in the sample volume and ellipticals the lowest.

The average density of galaxies appears to trend downwards at ~ 30 Mpc ($\mu + 5\log_{10}h = 32.38$ mag, $h = 1$), the maximum distance of the sample. The trend is not due to incompleteness for three reasons. First, the Rauzy test results described in Section 2.1. Second, $\mathrm{V/V}_{max} = 0.7$ in the outer shell ($31.88 \leq \mu + 5\log_{10}h \leq 32.38$ mag) indicating that the sample is complete up to the distance limit of the survey. Third, Choloniewski (1986) reported the same trend using an independent sample based on the CfA redshift survey. That sample revealed that the density increases again farther out at ~ 80 Mpc ($h = 1$) ($\mu + 5\log_{10}h = 34.51$ mag). Thus, the downward trend at the periphery of the K10/3000 sample is judged to be real and not symptomatic of a selection effect.

The decrease in galaxy density at 30 Mpc ($h = 1$) is large but within the plausible range of cosmic variance. An analytic estimate of cosmic variance (Davis & Huchra 1982) depends on the volume sampled and the galaxy two-point correlation function. The latter is not known directly for the K-selected sample, but we assume it's the same as for visually-

selected galaxy samples. A correlation function based on the fluctuation power spectrum from WMAP–1 (Spergel et al. 2003) was extrapolated to the present via the method of Seljak & Zaldarriaga (1996) then transformed via a spherical Bessel function and smoothed with a 1 Mpc radius (D. Eisenstein, private communication, 2006). The volume integral (e.g., Newman & Davis 2002, equation 1) was then evaluated via a Monte Carlo approach. The resulting cosmic variance uncertainty is ∼12% for the full sample and ∼18% for a sample half a magnitude less deep (Figure 6). The true correlation function is likely to be larger for K-selected galaxies, which are predominantly early-type, than for visually-selected ones, more of which are late-type (Figure 3). This suggests the preceding estimates may be too small. An alternate estimate for cosmic variance makes further use of the Millennium Simulation (Springel et al. 2005) and the semi-analytic galaxy catalog (De Lucia & Blaizot 2007; Croton et al. 2006). For this calculation, simulated galaxies were simply counted in 64 independent spheres of 30 and 23.8 Mpc ($h = 1$) radii, and standard deviations were 26% and 33% respectively of the mean galaxy density. These values would make the dip in the final bin of Figure 6 (or the excess in preceding bins) only about 2σ. The agreement of our overall luminosity function with that of Jones et al. (2006) (section 4.2) suggests that cosmic variance is not playing a large role in our results. Regardless of its magnitude, cosmic variance represents a single uncertainty for the entire LF, not an independent uncertainty in each luminosity bin, under the assumption that the LF is independent of location.

4.2. Parametric Fits to the K-band Luminosity Functions by Hubble Type

Figure 7 presents K-band LFs with Schechter function fits (Schechter 1976) for all galaxies and subsets segregated by morphological type. The LFs are defined in Table 3 and the corresponding Schechter function fit parameters are listed in Table 4. For the total K-band LF, values for the parameters $M_*-5\log_{10}h$, ϕ_*/h^3 and α agree within 2σ of previous determinations (Jones et al. 2006; Eke et al. 2005; Bell et al. 2003; Kochanek et al. 2001; Cole et al. 2001). We find a $\sim 40\%$ higher space density of galaxies in the range $-23 < \mathrm{M}_K-5\log_{10}h < -21$ mag than Jones et al. (2006) which represents a difference of about 2σ. Thus, unlike Jones et al. (2006), we do not find a residual with respect to the best fitting Schechter function over that magnitude interval.

Figure 7 shows that the K-band LF for ellipticals is represented by a Schechter function that declines toward both high and low luminosities, akin to the *red* elliptical sequence of Driver et al. (2007). Number counts decrease for low-luminosity elliptical galaxies until the low-luminosity upturn at $\mathrm{M}_K-5\log_{10}h > -21$ mag which represents the onset of the dwarf elliptical sequence at $M_B > -18$ (Sandage, Binggeli & Tammann 1985), akin to the *blue*

elliptical sequence of Driver et al. (2007).

The LFs for lenticular galaxies (S0) and bulge-dominated early-type spirals (S0/a - Sbc) are very similar and therefore have been combined. Like the ellipticals, the combined luminosity function for lenticulars and bulge-dominated spirals is represented by a Schechter function that declines toward both high and low luminosities. In contrast, the LF for late-type spirals (disk-dominated; types Sc–Scd) is completely different than found for the other galaxy types. Although this LF is also is well-represented by a Schechter function, the function is *essentially* a power law over the range of luminosities for which the LF can be defined, with a slope $\alpha = -1.4$ that predicts an increasing space density of low-luminosity late-type spirals with no evidence of a low luminosity turnover prior to $M_K - 5\log_{10}h < -19.75$ mag. An exponential turnover is expected at the high luminosity end.

Our findings with regard to the K-band LF are therefore threefold. First, we find a total LF that is consistent with previous work. Second, each of the three galaxy classes (ellipticals, bulge-dominated spirals, and disk-dominated late type spirals) have a LF with a distinct shape, and none of them mimics the shape of the total LF. Third, ellipticals dominate the space density at high luminosities, a result that is only accentuated if total magnitudes are considered (section 4.4), whereas late-type (Sc - Scd) spirals dominate the space density at low luminosities. Lying between these two extremes are the lenticular galaxies and the bulge-dominated spirals (S0/a - Sbc).

The only other study to have explored the morphological type dependence of K-band LFs is that of Kochanek et al. (2001). Using visual morphological classifications, they segregated their sample of bright, nearby galaxies ($K_{20} \leq 11.25$ mag, cz > 2000 km/s) into just two broad categories; early and late. Figure 8 illustrates the agreement between our results and those of Kochanek et al. (2001) when our sample is divided the same way as theirs, at $T = -0.5$, such that the early type sub-sample includes elliptical and lenticular galaxies and the late-type sub-sample includes all galaxies classified S0/a and later. The shape of the LFs are similar though not identical when galaxies are divided into these two broad categories. It is not until galaxies are more finely segregated that the differences between the LFs for the morphological types emerge.

4.3. K-band Luminosity Density by Hubble type

Calculating the luminosity density is important as it can provide a constraint on the mass density of stars in galaxies, given a mass to light ratio. Parameterizing the LFs allows the luminosity density j to be calculated by integration,

$$j = \int \phi(M) 10^{0.4(M_{\odot}-M)} dM \tag{3}$$

where $M_{\odot}$ is the absolute magnitude of the Sun, corresponding to 3.32 mag at K (Bell et al. 2003). The total K-band luminosity density was calculated by integrating equation 2 over the interval $-25 \leq M_K - 5\log_{10}h \leq -19$ mag using the Schechter function illustrated in Figure 7. This yields $(5.8 \pm 1.2) \times 10^8$ h $L_{\odot}$ Mpc $^{-3}$. A Monte Carlo method was used to calculate the uncertainty. Our value for the K-band total luminosity density agrees well with previous determinations (Jones et al. 2006; Bell et al. 2003; Kochanek et al. 2001; Cole et al. 2001), all of which are about a factor of two lower than the value reported by Huang et al. (2003). See Bell et al. (2003) for a discussion of the various luminosity density estimates in the literature.

Elliptical galaxies (Figure 7) contribute $\sim$16 $\pm$ 3% of the total K-band luminosity density of galaxies in the local universe. This value is revised upwards to $\sim$18% if total rather than isophotal magnitudes are considered (section 4.4). Lenticulars and bulge-dominated spirals (Figure 7) contribute $\sim$68$\pm$14% of the total, or $\sim$22 $\pm$ 4% for each sub-group (S0, S0/a–Sab, Sb–Sbc). Finally, the late-type spirals (Figure 7) contribute $\sim$16 $\pm$ 3% of the total. The results are summarized in Table 5. *To a good approximation, each Hubble type (E, S0, S0/a–Sab, Sb–Sbc, Sc–Scd) contributes equally to the overall K-band luminosity density in the local universe.*

4.4. K-band Bulge Luminosity Functions by Hubble type

In addition to the LFs for entire galaxies, the LF of bulges alone can provide information on how these structural components formed. For lenticular and spiral galaxies, it is possible, in principle, to decompose each galaxy into its bulge and disk components by modeling imaging data (e.g., Peng et al. 2002; Simard et al. 2002). An alternative approach, employed by Graham & Worley (2008), is to compute the bulge and disk luminosities from Sérsic bulge and exponential disk parameters. Graham & Worley (2008) have done this for a selection of about 400 nearby galaxies with K-band imaging in the published literature, many of which are in the K10/3000 sample. Thus, the resulting bulge/total luminosity ratios can be used statistically to predict bulge LFs for different Hubble types in the K10/3000 sample.

The total magnitudes adopted for spiral and lenticular galaxies are those reported in the 2MASS XSC under the parameter: `k_m_ext`. The total magnitudes were then corrected to bulge magnitudes using the bulge/total luminosity ratios as a function of morphological type reported in Graham & Worley (2008). Galaxies exhibit a range of bulge/total luminosity

ratios even within a particular morphological type. Following Graham & Worley (2008), the adopted 1σ ranges for $m_{bulge} - m_{total}$ are 1.12 to 2.18 mag for the S0–S0/a galaxies, 0.58 to 2.49 mag for the Sa–Sab galaxies, and 1.23 to 3.25 mag for the Sb–Sbc galaxies. A plausible bulge magnitude was estimated for each galaxy using a Monte Carlo method that applied a type specific $m_{bulge} - m_{total}$ correction to the total magnitude of each galaxy, randomly selected from a uniform distribution[5] of real numbers in the ranges quoted above. A bulge LF was then computed using the Choloniewski method. This procedure was repeated 55 times leading to an average LF and an associated standard deviation. The mean bulge LF and the 1σ standard deviation from the mean is reported in Table 6 for each morphological type.

Ellipticals do not have disks and so there is no $m_{bulge} - m_{total}$ correction. However, the 2MASS isophotal magnitudes for the ellipticals underestimate the total magnitudes due to the fact that a restriction was imposed on the value of the Sérsic index when the 2MASS total magnitudes were computed (Lauer et al. 2007). We determined the value $m_{iso} - m_{total}$ $= 0.44 \pm 0.28$ mag by comparing the 2MASS XSC K-band isophotal magnitudes with the total K-band magnitudes measured by Marconi & Hunt (2003) using GALFIT (Peng et al. 2002) for 14 ellipticals in the K10/3000 sample. We found no dependence of $m_{iso} - m_{total}$ with absolute K-band magnitude. Thus, total magnitudes are estimated by applying a correction, randomly selected from a uniform distribution of numbers in the range -0.16 to -0.72 mag, to the isophotal magnitude of each elliptical in the K10/3000 sample. Then a LF was computed using the Choloniewski method. This procedure was repeated 55 separate times leading to the average LF and the associated 1σ standard deviation reported for ellipticals in Table 6.

The derived bulge LFs, illustrated in Figure 9, predict that the K-band bulge LF is bimodal with the ellipticals clearly offset from the bulges of lenticulars and S0/a - Sbc spiral galaxies. This is a consequence of the type dependent *magnitude* corrections employed to obtain the bulge LFs. The corrections essentially shift the isophotal LFs (Figure 7) towards *higher* luminosities for the ellipticals and towards *lower* luminosites for the lenticulars and the S0/a - Sbc spiral galaxies, thereby accentuating the difference between the types already noted in section 4.2. Our combined bulge LF is similar in shape and amplitude to the B-band one reported by Driver et al. (2007), although a detailed comparison is complicated by the different wavelengths. The dwarf elliptical sequence *appears* to connect onto the

[5] It is not clear which distribution to adopt because $m_{bulge} - m_{total}$ has been measured for only a few galaxies in the K-band. However, similar results are obtained if a normal distribution is used instead of a uniform one. In either case, the mean correction affects the lateral displacement of the LF along the abscissa and the range of the correction affects the uncertainty which is reflected in the width of the band (Figure 9).

LFs for spiral bulges. However, our LF for dwarf ellipticals is incomplete, these objects have a distinct LF that continues to rise towards low luminosities as shown previously by Sandage, Binggeli & Tammann (1985).

Integrating the bulge LFs using equation 3 allows an estimate of the contribution of bulges to the K-band luminosity density in the local universe. The results are presented in Table 7. Interestingly, bulges in each of the Hubble types, S0–S0/a, Sa–Sab, and Sb–Sbc contribute approximately equally to the luminosity density. Ellipticals, on the other hand, contribute about 50% more to luminosity density than the lenticular and spiral bulges combined. Collectively, all bulges contribute $30 \pm 7\%$ of the total K-band luminosity density of galaxies in the local universe, thus the remaining $70 \pm 7\%$ is attributed to disks. A similar result was obtained previously in the V-band by Schechter & Dressler (1987).

5. Discussion

5.1. Morphological Type Dependence of the K-band Luminosity Function

Our principal new result is that the K-band isophotal LFs depend significantly on galaxy morphology. Broadly speaking, the K-band LFs for galaxies manifest in two varieties, both of which can be described mathematically by a Schechter function. The LFs for ellipticals, lenticulars and bulge-dominated spirals (S0/a - Sbc) are peaked with a fall-off at high and low luminosities. Although the functional forms for various types of *bulge* dominated galaxies are similar, the ellipticals are displaced about one magnitude brighter in luminosity compared to the lenticulars and bulge-dominated spirals, a difference that increases to $\sim$1.4 mag if total magnitudes are considered (section 4.4). In contrast, the disk-dominated late-type spirals (Sc–Scd) are distributed according to a power law with lower luminosity systems more numerous than any other galaxy type.

Overall, our results agree qualitatively with Binggeli, Sandage & Tammann (1988) and Loveday et al. (1992), who showed that the B-band LFs are different when galaxies are segregated by visible morphology. However, our results differ in detail, particularly with regard to the Sc galaxies. Subsequently, little evidence has been found for *type dependent* differences in the B–, SDSS– and 2MASS–band LFs for morphological types earlier than Sc–Scd (Efstathiou, Ellis, & Peterson 1988; Marzke et al. 1994, 1998; Kochanek et al. 2001; Nakamura et al., 2003). However, those galaxy samples were divided into two or at most three broad morphological classes whereas our results are based on a finer morphological segregation. Another factor to consider is the reliability of morphological assignments for distant galaxies. Morphological classification becomes difficult for distant and faint galaxies,

even more so when the morphological assignment is based on photographic Schmidt plates. As noted previously by de Lapparent (2003), variations among the LFs in the literature depend largely on the criteria employed for typing the galaxies and the subsequent grouping of types. When the different morphologies are bundled together the distinctions between the LFs become less apparent as Figure 8 illustrates. Our results are based on well resolved nearby galaxies, so the classifications are more dependable, and the distinctions revealed by our analysis resulted from dividing the galaxy sample into several morphological bins.

Given the difficulties with morphological classifications for distant galaxies one is compelled to critically evaluate the efficacy of surrogate but *quantitative* measures of galaxy morphology, such as the SDSS color and light concentration indices (Strateva et al. 2001), both of which yield significant differences in the resulting LFs (e.g., Blanton et al. 2001; Bell et al. 2003; Conselice 2003; Bell et al. 2004; Willmer et al. 2006; Blanton 2006; Faber et al. 2007). Finding the ideal combination of parameters that can also be applied to galaxy simulations is one of the current observational challenges. However subjective the visual classifications may be, their principal merit is that they do lead to distinct functional forms for the K-band LFs. Perhaps a useful compromise between the two approaches would be to classify galaxies using artificial neural networks (ANN), although this method too seems to have problems with ANN classifications leading to similar Schechter functions for all galaxy types (e.g., Ball et al. 2004, 2006). The Zurich Estimator of Structural Types (ZEST) is another approach introduced by Scarlata et al. (2007) that appears to do better by returning different forms for the LFs of *bulge* dominated and *disk* dominated galaxies that more closely resemble the distinctions revealed by our analysis.

The differing LFs for *bulge* dominated and *disk* dominated systems suggests at least two quite distinct galaxy formation mechanisms are at work to produce the diversity of morphological types seen in the local universe. The next step is to establish what the formation mechanisms are, which will require modeling the LFs in the context of hierarchical clustering scenarios (e.g., Cole et al. 2000; Benson et al. 2003). Semi-analytic models have revealed that a combination of cold gas accretion (Weinberg et al. 2004) and feedback (Oppenheimer & Davé 2006) can yield a mass function for galaxy disks that is similar to, but slightly flatter than, the slope of the halo mass function. Such models are also able to reproduce the peaked LFs observed for ellipticals and bulge-dominated spirals by incorporating major mergers (Barnes & Hernquist 1992; Hopkins et al. 2008b). Work already underway shows that the morphological dichotomy revealed by the K-band LFs can be understood within the context of galaxy evolution in ΛCDM cosmology (A. Benson & N. Devereux 2009, in preparation).

5.2. The Hubble Type Dependence of Black Hole Mass Functions

Most astronomers now believe that supermassive black holes (BHs) reside in the bulges of, possibly, all galaxies. The principal evidence is a correlation between the bulge luminosity, measured in the near-infrared, and black hole mass (Marconi & Hunt 2003; Ferrarese & Merritt 2000). The importance of this correlation is that the near-infrared luminosity of stellar bulges, a component on which the morphological classification of galaxies is based, may be used as a surrogate tracer of the extragalactic black hole mass function (BHMF) which in turn constrains physical models of black hole growth in the context of ΛCDM cosmology (Marconi et al. 2004; Hopkins et al. 2008a,b; Shankar, Weinberg & Miralda-Escudé 2009).

Using the group 1 calibration of Marconi & Hunt (2003), the bulge LFs shown in Figure 9 may be translated into BHMFs. When defining BHMFs this way, it is important to appreciate the following caveats. Firstly, the group 1 calibration of Marconi & Hunt (2003) is based primarily on elliptical galaxies, thus one has to assume that the same relation applies to lenticulars and the bulges of spirals[6]. Secondly, it has not yet been proven that BHs exist in *all* ellipticals, lenticulars and the bulges of *all* spirals, thus the derived space densities will be upper limits. Nevertheless, if BHs do exist in all bulges, and the same bulge luminosity - BH mass correlation holds for all, then our results predict that the BHMF is bimodal, and depends on Hubble type, with the ellipticals having a range of BH masses distinctly higher than the range of BH masses inhabiting lenticular and spiral galaxies. Our total BHMF is similar to other total BHMFs in the published literature which have been derived using a variety of relationships between BH mass and bulge properties. As summarized by Shankar, Weinberg & Miralda-Escudé (2009), many of the existing BHMF determinations are based on total galaxy LFs, which include all morphological types, with subsequent corrections for the contribution of each morphological type to the total LF, and a further correction to estimate the contribution of the spheroid to the luminosity of each type. Ours is the first to be based on LFs explicitly segregated by morphological type. With the aforementioned caveats in mind, our results further predict that the majority of BHs reside in lenticulars and the bulges of spirals. In contrast, the BHMF of Graham et al. (2007), which is based on an empirical non-linear relationship between BH mass and bulge Sérsic parameter, predicts a sharp decrease in the BHMF over that same interval (Figure 9). Which of these two vastly different predictions is correct hinges on whether the bulge luminosity (e.g., Marconi & Hunt 2003) or the bulge Sérsic parameter (e.g., Graham et al.

[6]Sc and later types have not been included in Figure 9 as central supermassive BHs have yet to be found in later type spirals (Gebhardt et al. 2001).

2007, and references therein) is the better predictor of the existence and mass of central BHs in lenticulars and the bulges of spiral galaxies.

Given the aforementioned caveats, an upper limit to the local mass density of BHs, $\rho_\bullet$, may be calculated by integrating the BHMFs using

$$\rho_\bullet = \int_{M_{lower}}^{M_{upper}} \phi(M_\bullet) M_\bullet d(log M_\bullet) \tag{4}$$

where $\phi(M_\bullet)$ is the differential BH mass function, mapped from the bulge LF (Figure 9), and $M_\bullet$ is the BH mass.

The result of the integral is very sensitive to the value of the upper mass limit which undoubtedly contributes to the factor of $\sim$2 range in estimates for $\rho_\bullet$ in the literature. Integrating between $6.5 \leq \log_{10}(M_{BH}) \leq 9.4$, where the upper mass limit corresponds to the highest *measured* BH mass (Kaspi et. al 2007) yields a total BH mass density of (4.6 ± 0.5) x 10^5 $M_\odot$ Mpc^{-3} ($h = 0.7$) in good agreement with previous determinations (Shankar, Weinberg & Miralda-Escudé 2009, and references therein). However, our prediction that the BHMF is bimodal associates over half, ($\sim 60\%$), of the total black hole mass density with elliptical galaxies, the bulges of spirals making up the remainder, apportioned approximately equally between the lenticulars, the S0/a-Sab's and the Sb-Sbc's.

At present, stellar bulges provide an efficient but indirect means of constraining supermassive black hole demographics without recourse to the difficult and time-consuming measurement of black hole masses *directly* using gas and star kinematics. In particular, because stellar bulge luminosities can be measured consistently for very large numbers of galaxies, the method has the potential to reduce biases that may affect other *indirect* methods, such as the use of broad emission lines (e.g. Greene & Ho 2007). We are currently undertaking the next logical step to refine this analysis which is to isolate the bulges explicitly using the 2MASS images.

6. Conclusions

K-band LFs have been presented for a complete volume limited sample of 1613 galaxies with $V_{gsr} \leq 3000\,km\,s^{-1}$, $K \leq 10$ mag and $|b| > 10$ degrees. Our principal conclusions are

1. The K-band LFs depend on morphological type when galaxies are segregated according to the visual classification scheme of de Vaucouleurs et al. (1991). Ellipticals dominate the space density at high luminosities whereas late-type spirals dominate the space density at

low luminosities. Lying in between the two extremes are the lenticulars and bulge-dominated spirals.

2. The K-band LF for late-type spirals follows a power law that rises towards low luminosities whereas the K-band LFs for ellipticals, lenticulars and bulge-dominated spirals are peaked with a falloff at both high and low luminosities.

3. Each morphological type (E, S0, S0/a–Sab, Sb–Sbc, Sc–Scd) contributes approximately equally to the overall K-band luminosity density in the local universe.

4. The K-band LF of bulges is bimodal and depends on morphological type. Ellipticals comprise 60% of the bulge luminosity density in the local universe, the remaining 40% is associated with lenticulars and the bulges of spirals. Overall, bulges contribute $\sim 30\%$ of the total galaxy luminosity density at K, with disks making up the difference.

5. If the bulge luminosity traces the black hole mass, our results predict that the black hole mass function is bimodal and depends on morphological type with the most massive black holes occurring in ellipticals and the space density of black holes reaching a maximum in the bulges of spirals.

N.D. gratefully acknowledges the support of the Fulbright Commission and the hospitality of the National University of Ireland, Galway, and the assistance of undergraduate students Meghan Burleigh, Sarah McNamara and Lisa Fallon for their help in the early stages of this project. Extensive use was made of the HyperLeda database (http://leda.univ-lyon1.fr) and data products from the Two Micron All Sky Survey, which is a joint project of the University of Massachusetts and the Infrared Processing and Analysis Center/California Institute of Technology, funded by the National Aeronautics and Space Administration and the National Science Foundation. The Millennium Simulation databases used in this paper and the web application providing online access to them were constructed as part of the activities of the German Astrophysical Virtual Observatory. We thank Darren Croton and Gerard Lemson for help with the database tools. We thank Daniel Eisenstein for supplying the galaxy correlation function used in the cosmic variance calculation. We thank John Huchra for providing galaxy redshifts in advance of publication and Alessandro Marconi and Francesco Shankar for digitized BHMFs.

Facilities: 2MASS

A. Appendix

This Appendix describes in detail how to calculate the size of the error bars on the differential LF ϕ(M), the number density of galaxies $\rho(\mu)$, and n, the average number density, where M is absolute magnitude and μ is the distance modulus. The reader is encouraged to consult Choloniewski (1986) prior to implementing the following strategy which requires a familiarity with the maximum-likelihood method of statistical analysis.

In order to characterize the statistical uncertainties on ϕ(M), $\rho(\mu)$, and n, the observables, M and μ, must be represented by a particular statistical model. Generally, this model is *assumed* to be a Poisson distribution, which means that the galaxies are distributed independently of position, that the average number of galaxies in a region of space is proportional only to the volume of that region, and that their luminosities are uncorrelated with their locations. This model yields the familiar and widely adopted result $1/(2.3\sqrt{N})$ for the uncertainty in $\log_{10}\phi$(M), where N is the number of galaxies in the absolute magnitude interval, ΔM. However, it is rarely, if ever, proven that the observables, M and μ, *are* distributed in a Poisson fashion even though there are reasons to believe that this may not be a good assumption given the clustering tendencies for elliptical galaxies in particular. We have discovered, in the course of writing this paper, that some uncertainties calculated using the procedure described below are less than $1/2.3\sqrt{N}$. These cases are indicated by asterisks in Table 3. This outcome suggests that the galaxy distribution is not Poisson, but is instead slightly clumped in space and luminosity and better represented by a *generalized Poisson distribution* (Consul 1989). The *generalized Poisson* distribution is described by

$$p(N|V,b) = \frac{\bar{N}(1-b)}{N!}[\bar{N}(1-b)+Nb]^{N-1}e^{-\bar{N}(1-b)-Nb}. \quad \text{(A1)}$$

Here $p(N|V,b)$ is the probability that a cell of volume V placed randomly in space contains exactly N galaxies. If n is the average density of galaxies then $\bar{N} = \mathrm{n}V$. An application of this distribution to hierarchical clustering is described by Sheth (1998) and Saslaw & Hamilton (1984). A formal analysis, similar to that outlined below, but beyond the scope of the present paper, would constrain the parameter b to the range $0 \leq b \leq 1$ with the standard Poisson distribution corresponding to the case $b = 0$. Such a distribution would yield uncertainties that are larger than $1/2.3\sqrt{N}$ by a factor $1/(1-b)$.

Following Choloniewski (1986), we proceed with the Poisson distribution function, and adopt the notation of Choloniewski (1986), which is most easily understood with reference to Figure 2 of that paper. A is the total number of absolute magnitude columns, indexed by the counter i, and B is the total number of distance modulus rows, indexed by the counter j. A magnitude limited sample fills the M, μ plane only partially, in the region below the selection line $\mathrm{M} + \mu = \mathrm{m}_{lim}$, where m_{lim} is the magnitude limit of the survey. The parameter

S, is the magnitude limit of the survey, m_{lim}, in units of i and j, such that $i + j \leq$ S, an inequality because the galaxies are also contained within a finite volume and within a finite range of absolute magnitudes.

The covariance, a matrix whose leading diagonal contains the uncertainties for the values, ϕ_i, ρ_j, n, can be approximated by use of the information matrix, specifically,

$$Cov(\hat{E}) \approx \left[-\frac{\partial^2 ln(l)}{\partial E^2} \right]^{-1}_{E=\hat{E}} \tag{A2}$$

where l is the likelihood function, which is chosen to be Poisson. The minus sign corrects a typo in Choloniewski (1986), (see Eadie 1982). Following Choloniewski (1986), $E = (\phi_i, \rho_j, n)$, are called the *estimators* and are the computed values defining ϕ(M), the differential LF, where M is absolute magnitude, $\rho(\mu)$, the number density of galaxies as a function of distance modulus, μ, and n, the average number density of galaxies in the sample.

The Hessian $\frac{\partial^2 ln(l)}{\partial E^2}$ of l can be written as a 3 by 3 symmetric matrix with each entry itself a matrix:

$$\frac{\partial^2 ln(l)}{\partial E^2} = \begin{bmatrix} \frac{\partial^2 ln(l)}{\partial \phi^2} & \frac{\partial^2 ln(l)}{\partial \phi \partial \rho} & \frac{\partial^2 ln(l)}{\partial \phi \partial n} \\ \frac{\partial^2 ln(l)}{\partial \rho \partial \phi} & \frac{\partial^2 ln(l)}{\partial \rho^2} & \frac{\partial^2 ln(l)}{\partial \rho \partial n} \\ \frac{\partial^2 ln(l)}{\partial n \partial \phi} & \frac{\partial^2 ln(l)}{\partial n \partial \rho} & \frac{\partial^2 ln(l)}{\partial n^2} \end{bmatrix}. \tag{A3}$$

So, the next step in the procedure is clear, but complicated, because it entails taking the second derivative of the likelihood function with respect to each of the variables, ϕ_i, ρ_j and n.

The Poisson likelihood function is given by

$$l = \prod_{\substack{i=1 \\ i+j \leq S}}^{A} \prod_{j=1}^{B} e^{-\lambda_{i,j}} \frac{\lambda_{i,j}^{N_{i,j}}}{N_{i,j}!} \tag{A4}$$

where $\lambda_{i,j} = \frac{1}{n}\phi_i \Delta M \rho_j (V_j - V_{j-1})$, and V is the sample volume and ΔM is the magnitude interval.

Taking the natural log we obtain,

$$ln(l) = \sum_{\substack{i=1 \\ i+j \leq S}}^{A} \sum_{j=1}^{B} e^{-\lambda_{i,j}} \frac{\lambda_{i,j}^{N_{i,j}}}{N_{i,j}!} - \lambda_{i,j} + N_{i,j} ln(\lambda_{i,j}) - ln(N_{i,j}!) \tag{A5}$$

Unless otherwise stated double products such as $\prod_{\substack{i=1 \\ i+j \leq S}}^{A} \prod_{j=1}^{B}$ will be denoted by $\prod_{i+j \leq S}$ and double sums such as $\sum_{\substack{i=1 \\ i+j \leq S}}^{A} \sum_{j=1}^{B}$ will be denoted by $\sum_{i+j \leq S}$.

Here $N_{i,j}$ = the number of galaxies in bin i,j. Consequently

$$\frac{\partial N_{i,j}}{\partial \phi_k} = \frac{\partial N_{i,j}}{\partial \rho_k} = \frac{\partial N_{i,j}}{\partial n} = 0. \tag{A6}$$

For the first sub-matrix,

$$\frac{\partial^2 ln(l)}{\partial \phi^2} = \begin{bmatrix} \frac{\partial^2 ln(l)}{\partial \phi_1 \partial \phi_1} & \cdots & \cdots \\ \vdots & \frac{\partial^2 ln(l)}{\partial \phi_i \partial \phi_j} & \vdots \\ \vdots & \cdots & \ddots \end{bmatrix}. \tag{A7}$$

We have

$$\frac{\partial^2 ln(l)}{\partial \phi_i \partial \phi_j} = \frac{\partial^2}{\partial \phi_i \partial \phi_j} \left(\sum_{\alpha+\beta \leq S} -\lambda_{\alpha\beta} + N_{\alpha\beta} ln(\lambda_{\alpha\beta}) - ln(N_{\alpha\beta}!) \right). \tag{A8}$$

By definition $\lambda_{\alpha\beta} = \frac{1}{n}\phi_\alpha \Delta M \rho_\beta (V_\beta - V_{\beta-1})$, where V is the sample volume and ΔM is the magnitude interval. We introduce new dummy variables α, β which are independent of the variables i, j. This is necessitated by the need to distinguish between the variables which the likelihood is a function of and the factors which the likelihood is composed of.

Letting $C_\beta = \Delta M (V_\beta - V_{\beta-1})$, this becomes $\lambda_{\alpha\beta} = C_\beta \frac{1}{n} \phi_\alpha \rho_\beta$, and so

$$\frac{\partial \lambda_{\alpha\beta}}{\partial \phi_i} = \begin{array}{lll} 0 & \text{if} & \alpha \neq i, \\ C_\beta \frac{1}{n} \rho_\beta & \text{if} & \alpha = i. \end{array} \tag{A9}$$

So $\frac{\partial^2 \lambda_{\alpha\beta}}{\partial \phi_i \partial \phi_j} = 0$ for all α, β, i, j. Also $\frac{\partial^2 N_{\alpha\beta}!}{\partial \phi_i \partial \phi_j} = 0$ for all α, β, i, j. Consequently

$$\frac{\partial^2 ln(l)}{\partial \phi_i \partial \phi_j} = \frac{\partial^2}{\partial \phi_i \partial \phi_j} \left(\sum_{\alpha+\beta \leq S} N_{\alpha\beta} ln(\lambda_{\alpha\beta}) \right). \tag{A10}$$

Now

$$\frac{\partial}{\partial \phi_j} \left(\sum_{\alpha+\beta \leq S} N_{\alpha\beta} ln(\lambda_{\alpha\beta}) \right) = \sum_{\alpha+\beta \leq S} N_{\alpha\beta} \frac{\partial ln(\lambda_{\alpha\beta})}{\partial \phi_j}. \tag{A11}$$

$$= \sum_{\alpha+\beta \leq S} N_{\alpha\beta} \frac{\partial ln(C_\beta \frac{1}{n} \phi_\alpha \rho_\beta)}{\partial \phi_j} \tag{A12}$$

$$= \sum_{\beta=1}^{S-j} N_{j\beta} \frac{\partial ln(C_\beta \frac{1}{n} \phi_j \rho_\beta)}{\partial \phi_j} = \sum_{\beta=1}^{S-j} N_{j\beta} \frac{1}{\phi_j}. \tag{A13}$$

So

$$\frac{\partial^2 ln(l)}{\partial\phi_i\partial\phi_j} = \frac{\partial}{\partial\phi_i}\sum_{\beta=1}^{S-j} N_{j\beta}\frac{1}{\phi_j} \tag{A14}$$

$$= \sum_{\beta=1}^{S-j} N_{j\beta}\frac{\partial(\phi_j^{-1})}{\partial\phi_i} \tag{A15}$$

$$= \begin{array}{ll} \frac{-1}{\phi_i^2}\sum_{\beta=1}^{S-i} N_{i\beta} & \text{if } i=j, \\ 0 & \text{if } i\neq j \end{array} \tag{A16}$$

Replacing the dummy variable β by the variable j we obtain

$$\frac{\partial^2 ln(l)}{\partial\phi_i\partial\phi_j} = \begin{array}{ll} \frac{-1}{\phi_i^2}\sum_{j=1}^{S-i} N_{ij} & \text{if } i=j, \\ 0 & \text{if } i\neq j \end{array} \tag{A17}$$

Therefore the first block of the Hessian matrix is an A x A matrix

$$\left[\ \frac{\partial^2 ln(l)}{\partial\phi^2}\ \right] = \begin{bmatrix} \frac{-\sum_{j=1}^{S-1} N_{1j}}{\phi_i^2} & 0 & 0 \\ 0 & \frac{-\sum_{j=1}^{S-2} N_{2j}}{\phi_i^2} & 0 \\ 0 & 0 & \ddots \end{bmatrix}. \tag{A18}$$

in which all terms are zero, except the leading diagonal, which is just the sum of the galaxies in each column, i, divided by -ϕ_i^2.

We next calculate $\frac{\partial^2 ln(l)}{\partial\rho_i\partial\rho_j}$. Since $\lambda_{\alpha\beta} = C_\beta\frac{1}{n}\phi_\alpha\rho_\beta$,

$$\frac{\partial\lambda_{\alpha\beta}}{\partial\rho_j} = \begin{array}{lll} 0 & \text{if} & \beta\neq j, \\ C_j\frac{1}{n}\phi_\alpha & \text{if} & \beta = j. \end{array} \tag{A19}$$

Therefore $\frac{\partial^2\lambda_{\alpha\beta}}{\partial\rho_i\partial\rho_j} = 0$ for all i, j, α, β and

$$\frac{\partial^2 ln(l)}{\partial\rho_i\partial\rho_j} = \frac{\partial^2}{\partial\rho_i\partial\rho_j}\sum_{\alpha+\beta\leq S} N_{\alpha\beta} ln(\lambda_{\alpha\beta}). \tag{A20}$$

One has

$$\frac{\partial}{\partial\rho_j}\sum_{\alpha+\beta\leq S} N_{\alpha\beta} ln(\lambda_{\alpha\beta}) = \sum_{\alpha+\beta\leq S} N_{\alpha\beta}\frac{\partial}{\partial\rho_j} ln(\lambda_{\alpha\beta}) = \sum_{\alpha=1}^{S-j} N_{\alpha j}\frac{\partial}{\partial\rho_j} ln(C_\beta\frac{1}{n}\phi_\alpha\rho_j) \tag{A21}$$

$$= \sum_{\alpha=1}^{S-j} N_{\alpha j}\frac{\partial}{\partial\rho_j}(ln(C_\beta\frac{1}{n}\phi_\alpha) + ln(\rho_j)) = \sum_{\alpha=1}^{S-j}\frac{N_{\alpha j}}{\rho_j}. \tag{A22}$$

Therefore

$$\frac{\partial^2 ln(l)}{\partial\rho_i\partial\rho_j} = \frac{\partial}{\partial\rho_i}\sum_{\alpha=1}^{S-j}\frac{N_{\alpha j}}{\rho_j} \tag{A23}$$

$$= \begin{array}{ll} 0 & \text{if } i \neq j, \\ \sum_{\alpha=1}^{S-j}(\frac{-N_{\alpha j}}{\rho_j^2}) & \text{if } i = j. \end{array} \tag{A24}$$

$$= \begin{array}{ll} 0 & \text{if } i \neq j, \\ \frac{-\sum_{i=1}^{S-j} N_{ij}}{\rho_j^2} & \text{if } i = j. \end{array} \tag{A25}$$

To summarize, the next block of the Hessian matrix is a B x B matrix

$$\left[\ \frac{\partial^2 ln(l)}{\partial\rho\partial\rho}\ \right] = \begin{bmatrix} -\frac{\sum_{i=1}^{S-1} N_{i1}}{\rho_1^2} & 0 & 0 \\ 0 & \frac{-\sum_{i=1}^{S-2} N_{i2}}{\rho_2^2} & 0 \\ 0 & 0 & \ddots \end{bmatrix}. \tag{A26}$$

in which all terms are zero, except the leading diagonal, which is just the sum of the galaxies in each row, j, divided by -ρ_j^2.

To calculate $\frac{\partial^2 ln(l)}{\partial n^2}$ we proceed as follows: Since $\lambda_{\alpha\beta} = C_\beta \frac{1}{n}\phi_\alpha\rho_\beta$,

$$\frac{\partial\lambda_{\alpha\beta}}{\partial n} = -C_\beta n^{-2}\phi_\alpha\rho_\beta, \tag{A27}$$

hence

$$\frac{\partial^2\lambda_{\alpha\beta}}{\partial n^2} = 2C_\beta n^{-3}\phi_\alpha\rho_\beta, \tag{A28}$$

and

$$\frac{\partial^2}{\partial n^2}\sum_{\alpha+\beta\leq S} -\lambda_{\alpha\beta} = -2\left(\sum_{\alpha+\beta\leq S} C_\beta\phi_\alpha\rho_\beta\right)n^{-3}. \tag{A29}$$

Also

$$\frac{\partial^2 ln(\lambda_{\alpha\beta})}{\partial n^2} = \frac{\partial^2}{\partial n^2}\left(ln(C_\beta\phi_\alpha\rho_\beta) - ln(n)\right) = -\frac{\partial^2}{\partial n^2}\left(ln(n)\right) = n^{-2}. \tag{A30}$$

Consequently

$$\frac{\partial^2 ln(l)}{\partial n^2} = -2\left(\sum_{\alpha+\beta\leq S} C_\beta\phi_\alpha\rho_\beta\right)n^{-3} + \left(\sum_{\alpha+\beta\leq S} N_{\alpha\beta}\right)n^{-2} \tag{A31}$$

$$= -2\frac{\sum_{i+j\leq S} C_j\phi_i\rho_j}{n^3} + \frac{\sum_{i+j\leq S} N_{ij}}{n^2}. \tag{A32}$$

a single scalar term.

We next calculate the first of the cross terms, $\frac{\partial^2 ln(l)}{\partial\phi\partial\rho}$.

Since $\lambda_{\alpha\beta} = C_\beta \frac{1}{n}\phi_\alpha\rho_\beta$,

$$\frac{\partial\lambda_{\alpha\beta}}{\partial\rho_j} = \begin{array}{ll} 0 & \text{if } \beta \neq j, \\ C_j\frac{1}{n}\phi_\alpha & \text{if } \beta = j. \end{array} \tag{A33}$$

then

$$\frac{\partial^2\lambda_{\alpha\beta}}{\partial\phi_i\partial\rho_j} = \begin{array}{ll} 0 & \text{if } \beta \neq j, \\ \frac{\partial}{\partial\phi_i}C_j\frac{1}{n}\phi_\alpha & \text{if } \beta = j. \end{array} \tag{A34}$$

$$= \begin{array}{ll} 0 & \text{if } \beta \neq j \text{ or } \alpha \neq i, \\ C_j\frac{1}{n} & \text{if } \beta = j \text{ and } \alpha = i. \end{array} \tag{A35}$$

Since

$$\frac{\partial^2 ln(\lambda_{\alpha\beta})}{\partial\phi_i\partial\rho_j} = \frac{\partial^2}{\partial\phi_i\partial\rho_j}\left(lnC_\beta - ln(n) + ln\phi_\alpha + ln\rho_\beta\right) = \frac{\partial}{\partial\phi_i}\left(0 - 0 + \frac{\partial ln\phi_\alpha}{\partial\rho_j} + \frac{ln\rho_b}{\partial\rho_j}\right) = 0. \tag{A36}$$

Consequently $\frac{\partial^2 ln(l)}{\partial\phi_i\partial\rho_j} = -\sum_{\alpha+\beta\leq S}\frac{\partial^2\lambda_{\alpha\beta}}{\partial\phi_i\partial\rho_j}$

$$= \begin{array}{ll} \frac{C_j}{n} & \text{if } i+j \leq S, \\ 0 & \text{otherwise.} \end{array} \tag{A37}$$

Therefore:

$$\frac{\partial^2 ln(l)}{\partial\phi\partial\rho} = \begin{bmatrix} -C_1/n & -C_1/n & -C_1/n & \cdots & C_1/n & C_1/n \\ -C_2/n & -C_2/n & -C_2/n & \cdots & C_2/n & C_2/n \\ -C_3/n & -C_3/n & -C_3/n & \cdots & C_3/n & C_3/n \\ -C_4/n & -C_4/n & -C_4/n & \cdots & C_4/n & 0 \\ -C_5/n & -C_5/n & -C_5/n & \cdots & 0 & 0 \\ \cdots & \cdots & \cdots & 0 & 0 & 0 \\ \cdots & \cdots & 0 & 0 & 0 & 0 \\ -C_B/n & \cdots & 0 & 0 & 0 & 0 \end{bmatrix}. \tag{A38}$$

a B x A array, and its reflection, $\frac{\partial^2 ln(l)}{\partial\rho\partial\phi}$, an A x B array.

To calculate the next cross term $\frac{\partial^2 ln(l)}{\partial\phi\partial n}$:

$$\frac{\partial\lambda_{\alpha\beta}}{\partial n} = -C_\beta n^{-2}\phi_\alpha\rho_\beta, \tag{A39}$$

so

$$\frac{\partial^2\lambda_{\alpha\beta}}{\partial\phi_i\partial n} = \begin{array}{ll} 0 & \text{if } \alpha \neq i, \\ \frac{-C_\beta\rho_\beta}{n^2} & \text{if } \alpha = i. \end{array} \tag{A40}$$

Therefore

$$\frac{\partial^2}{\partial\phi_i\partial n}\sum_{\substack{\alpha=1\\ \alpha+\beta\le S}}^{A}\sum_{\beta=1}^{B}\lambda_{\alpha\beta}=\sum_{\beta=1}^{B\wedge(S-i)}\frac{\partial^2\lambda_{\alpha\beta}}{\partial\phi_i\partial n}=-\frac{\sum_{\beta=1}^{B\wedge(S-i)}C_\beta\rho_\beta}{n^2}. \tag{A41}$$

(where $x\wedge y$ denotes $min(x,y)$).

$$\frac{\partial^2 ln\lambda_{ij}}{\partial\phi_i\partial n}=\frac{\partial^2}{\partial\phi_i\partial n}\left(lnC_\beta-ln(n)+ln\phi_\alpha+ln\rho_\beta\right)=0-\frac{\partial}{\partial\phi_i}\frac{1}{n}+0+0=0. \tag{A42}$$

So

$$\frac{\partial^2 ln(l)}{\partial\phi_i\partial n}=\frac{\sum_{j=1}^{B\wedge(S-i)}C_j\rho_j}{n^2} \tag{A43}$$

and

$$\frac{\partial^2 ln(l)}{\partial\phi\partial n}=\left(\frac{\sum_{j=1}^{B\wedge(S-1)}C_j\rho_j}{n^2},\frac{\sum_{j=1}^{B\wedge(S-2)}C_j\rho_j}{n^2}\cdots,\frac{\sum_{j=1}^{B\wedge(S-A)}C_j\rho_j}{n^2}\right) \tag{A44}$$

a column vector, and its reflection, $\frac{\partial^2 ln(l)}{\partial n\partial\phi}$, a row vector, each containing A terms.

Now, the final cross term,

$$\frac{\partial^2 ln(l)}{\partial\rho_j\partial n} \tag{A45}$$

Since

$$\frac{\partial\lambda_{\alpha\beta}}{\partial n}=-C_\beta n^{-2}\phi_\alpha\rho_\beta, \tag{A46}$$

$$\frac{\partial^2\lambda_{\alpha\beta}}{\partial\rho_j\partial n}=\begin{array}{ll}0 & \text{if } \beta\neq j,\\ \frac{-C_\beta\phi_\alpha}{n^2} & \text{if } \beta=j.\end{array} \tag{A47}$$

So

$$\frac{\partial^2}{\partial\rho_j\partial n}\sum_{\substack{\alpha=1\\ \alpha+\beta\le S}}^{A}\sum_{\beta=1}^{B}\lambda_{\alpha\beta}=-\frac{\sum_{\alpha=1}^{A\wedge(S-j)}C_j\phi_\alpha}{n^2}=-C_j\frac{\sum_{\alpha=1}^{A\wedge(S-j)}\phi_\alpha}{n^2}=-C_j\frac{\sum_{i=1}^{A\wedge(S-j)}\phi_i}{n^2}. \tag{A48}$$

To calculate $\frac{\partial^2 ln\lambda_{\alpha\beta}}{\partial\rho_j\partial n}$:

$$\frac{\partial ln\lambda_{\alpha\beta}}{\partial n}=\frac{\partial}{\partial n}\left(lnC_\beta-ln(n)+ln\phi_\alpha+ln\rho_\beta\right)=-\frac{1}{n}. \tag{A49}$$

So

$$\frac{\partial^2 ln(\lambda_{\alpha\beta})}{\partial\rho_j\partial n}=-\frac{\partial 1/n}{\partial\rho_j}=0. \tag{A50}$$

Thus,

$$\frac{\partial^2 ln(l)}{\partial \rho_j \partial n} = C_j \frac{\sum_{i=1}^{S-j} \phi_i}{n^2}. \tag{A51}$$

So, the last block of the Hessian matrix is,

$$\left(C_1 \frac{\sum_{i=1}^{A\wedge(S-1)} \phi_i}{n^2}, ..., C_B \frac{\sum_{i=1}^{A\wedge(S-B)} \phi_i}{n^2} \right) \tag{A52}$$

another column vector, and its reflection, $\frac{\partial^2 ln(l)}{\partial n \partial \rho}$, a row vector, each containing B terms.

Finally, take the inverse of the negative of the $(A + B + 1)$ x $(A + B + 1)$ Hessian matrix, the leading diagonal of which contains the uncertainties on ϕ(M), $\rho(\mu)$, and n.

REFERENCES

Andreon, S., 2002, A&A, 382, 495

Ball, N.M., Loveday, J., Fukugita, M., Nakamura, O., Brinkman, J., & Brunner, R.J., 2004, MNRAS, 348, 1048

Ball, N.M., Loveday, J., Brunner, R.J., Baldry, I.K., & Brinkman, J., 2006, MNRAS, 373, 845

Balland, C., Silk, J., & Schaeffer, R. 1998, ApJ, 497, 541

Barnes, J.E., & Hernquist, L., 1992, ARA&A, 30, 705

Bell, E. F., et al. 2004, ApJ, 608, 752

Bell, E.F., & de Jong, R.S., 2001, MNRAS, 312, 497

Bell, E.F., McIntosh, D.H., Katz, N., & Weinberg, M.D, 2003, ApJS, 149, 289

Benson, A.J., Bower, R.G., Frenk, C.S, Lacey, C.G., Baugh, C.M., & Cole, S, 2003, ApJ, 599, 38

Bingelli, G.A., Sandage, A., & Tammann, B.,1988, ARA&A, 26, 509

Blanton, M.R., 2006, ApJ, 648, 268

Blanton, M.R., et al., 2001, AJ, 121, 2358

Blanton, M. R., et al., 2003, ApJ, 592, 819

Brown, M. J. I., et al., 2007, ApJ, 654, 858

Choloniewski, J., 1986, MNRAS, 223,1

Cole, S., et al., 2000, MNRAS, 319, 168

Cole, S., et al., 2001, MNRAS, 326, 255

Conselice, C.J., 2003 ApJS, 147, 1

Consul, P.C., 1989, Generalized Poisson Distributions: Properties and Applications, Marcel Dekker Inc., New York, Basel

Croton, D. J., et al., 2006, MNRAS, 365, 11

Davis, M. & Huchra, J., 1982, ApJ, 254, 437.

de Lapparent, V., 2003, A&A, 408, 845

De Lucia, G., & Blaizot, J. 2007, MNRAS, 375, 2

de Vaucouleurs, G., 1959, *Handbuch der Physik*, 53, 275 (Berlin: Springer Verlag)

de Vaucouleurs, G., de Vaucouleurs, A., Corwin, H.G., Buta, R. J., Paturel, G., Fouque, P., 1995, *Third Reference Catalog of Bright Galaxies*, (New York: Springer Verlag)

Devereux, N.A., Becklin, E.E., & Scoville, N.Z., 1987, ApJ, 312, 529

Dressler, A., 1980, ApJ, 236, 351

Driver, S.P., Allen, P.D., Liske, J., & Graham, A.W., 2007, ApJ, 657, 85

Eadie,W.T., Drijard, D., James, F.E., Roos, M., Sadoulet, B., 1982, Statistical Methods in Experimental Physics, North Holland Publishing Company, Netherlands

Efstathiou, G., Ellis, R. S., Peterson, B. A., 1988, MNRAS, 232, 431

Eke, V.R., Baugh, C.M., Cole, S., Frenk, C.S., King, H.M., Peacock, J.A., 2005, MNRAS, 362, 1233

Faber, S. M., et al., 2007, ApJ, 665, 265

Ferrarese, L., & Merritt, D., 2000, ApJ, 539, 9

Freedman, W.L., et al. 2001, ApJ, 553, 47

Gebhardt, K., et al. 2001, AJ, 122, 2469

Graham, A.W., & Worley, C.C., 2008 MNRAS, 388, 1708

Graham, A.W., Driver, S.P., Allen, P.D., & Liske, J., 2007, MNRAS, 378, 198.

Greene, J. E. & Ho, L. C., 2007, ApJ, 667, 131

Huang, J.-S., Glazebrook, K., Cowie, L.L., & Tinney, C., 2003, ApJ, 584, 203

Hopkins, P.F., Hernquist, L., Cox, T.J., & Keres, D., 2008a, ApJS, 175, 356

Hopkins, P.F., Cox, T.J., Keres, D.,& Hernquist, L., 2008b, ApJS, 175, 390

Hubble, E., 1936, Realm of the Nebulae (New Haven: Yale University Press).

Ilbert, O., et al. 2005, A&A, 439, 863

Jarrett, T. H., Chester, T., Cutri, R., Schneider, S., Skrutskie, M., Huchra, J. P., 2000, AJ, 119, 2498

Jarrett, T.H., et al., 2003, AJ, 125, 525

Jones, D.H., Peterson, B.A., Colless, & Saunders, W., 2006, MNRAS, 369, 25

Karachentsev, I.D., Mitronova, S.N., Karachentseva, V.E., Kudrya, Y, N., & Jarrett, T.H., 2002, A&A, 396, 431

Karachentsev, I.D., 2004, AJ, 127, 2031

Karachentsev, I.D., 2006, AJ, 131, 1361

Kaspi, S., Brandt, W.N., Maoz, D., Netzer, H., Schneider, D.P., & Shemmer, 2007, ApJ, 659, 997

Kochanek, C. S., Pahre, M. A., Falco, E. E., Huchra, J. P., Mader, J., Jarrett, T. H., Chester, T., Cutri, R., Schneider, S. E., 2001, ApJ, 560, 566

Lauer, T., et al., 2007, ApJ, 662, 808

Loveday, J., Peterson, B.A., Efstathiou, G., & Maddox, S.J., 1992, ApJ, 390, 338

Lynden-Bell, D., Faber, S. M., Burstein, D., Davies, R. L., Dressler, A.,Terlevich, R. J., & Wegner, G., 1988, ApJ, 326, 19

Kormendy, J., Fisher, D.B., Cornell, M.E., & Bender, R., 2008, ApJS, in press

Marconi, A., & Hunt, L. K., 2003, ApJ, 589, 21.

Marconi, A., Risaliti, G., Gilli, R., Hunt, L. K., Maiolino, R., & Salvati, M., 2004, MNRAS, 351, 169.

Marzke, R.O., Geller, M.J., Huchra, J.P., & Corwin, H.G.,1994, AJ, 108, 437.

Marzke, R.O., Da Costa, L.N., Pellegrini, P.S., Willmer, C.N.A., & Geller, M.J., 1998, ApJ, 503, 617

Nakamura, O., et al., 2003, AJ, 125, 1682.

Newman, J. A. & Davis, M., 2002, ApJ, 564, 567

Norberg, P., et al. 2002, MNRAS, 332, 827

Oppenheimer, B. D., & Davé, R., 2006, MNRAS, 373, 1265

Paturel, G., Petit, C., Prugniel, Ph., Theureau, G., Rousseau, J., Brouty, M., Dubois, P., Cambrésy, L., 2003, A&A, 412, 45

Peng, C., Y., Ho, L. C., Impey, C. D., Rix, H-W., 2002, AJ, 124, 266.

Rauzy, S., 2001, MNRAS, 324, 51

Reddy, N. A., et al., 2008, ApJS, 175, 48

Sandage, A., Tammann, G. A., & Yahil, A., 1979 ApJ, 232, 352

Sandage, A., Binggeli , B., & Tammann, G. A., 1985, AJ, 90, 1759

Saslaw, W.C., & Hamilton, A.J.S., 1984, ApJ, 276, 13

Scarlata, C., et al., 2007, ApJS, 172, 406

Schechter, P., 1976, ApJ, 203, 297

Schechter, P., & Dressler, A., 1987, AJ, 94, 563

Skrutskie, M.F., et al., 2006, AJ, 131, 1163

Seljak, U., & Zaldarriaga, M., 1996, ApJ, 469, 437

Shankar, F.,Weinberg, D.H., & Miralda-Escudé, J., 2009, ApJ, 690, 205

Shaya, E., 1995, ApJ, 454, 15

Sheth, R., 1998, MNRAS, 299, 207

Simard, L., et al., 2002, ApJS, 142, 1

Spergel, D. N., et al., 2003, ApJS, 148, 175

Springel, V., et al., 2005, Nature, 435, 629

Strateva, I., et al., 2001, AJ, 122, 1861

Takeuchi, T. T., Yoshikawa, K., & Ishii, T. T. 2000, ApJS, 129, 1

Tonry, J., et al., 2001, ApJ, 546, 681

Tully, R. B., Fisher, J. R, 1977 A&A, 54, 661.

Tully, R.B., Shaya, E. J., Karachentsev, I. D., Courtois, H. M., Kocevski, D. D., Rizzi, L., Peel, A., 2008, ApJ, 676, 184.

Wake, D. et al. 2006, MNRAS, 372, 537

Weinberg, D.H., Dave, R., Katz, N., & Hernquist, L., ApJ, 601, 1

Willmer, C. N. A., et al. 2006, ApJ, 647, 853

Willmer, C.N.A., 1997, AJ, 114, 898

Wolf, C., et al. 2003, A&A, 401, 73

York, D., et al., 2000, AJ, 120, 1579

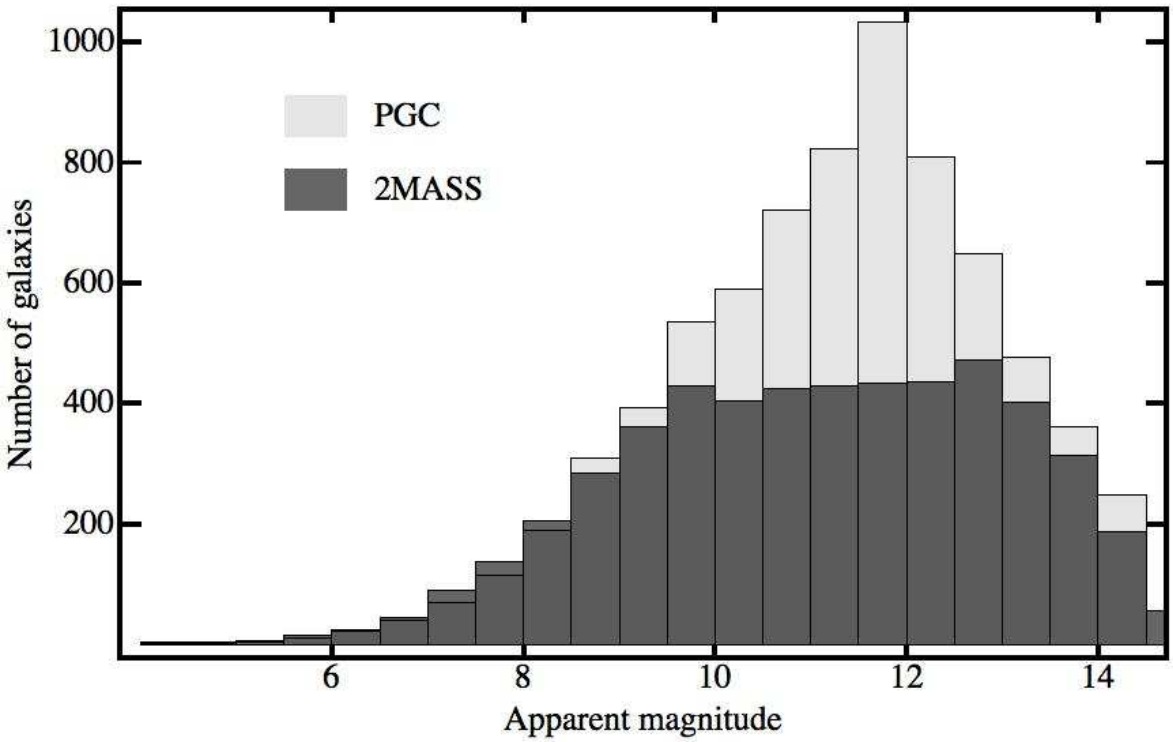

Fig. 1.— Histograms showing the distribution of B −3.5 magnitudes for a sample of 7406 nearby PGC galaxies ($V_{gsr} \leq 3000\,km\,s^{-1}$, $|b| > 10^o$, $m_B \leq 18$ mag) and the distribution of K-band magnitudes for the subset of 5034 in the same volume that appear in the 2MASS XSC, and from which the K10/3000 galaxy sample is selected.

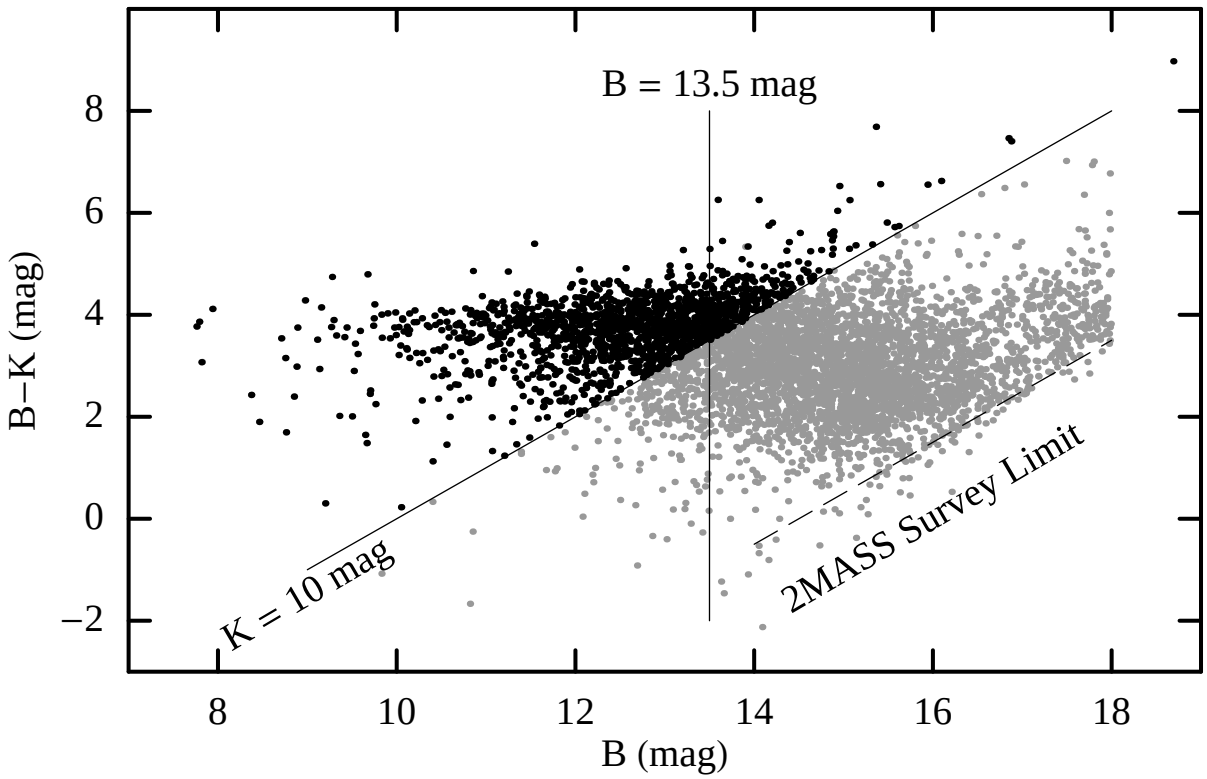

Fig. 2.— B−K color versus apparent B magnitude for 5034 nearby PGC galaxies in the 2MASS XSC ($V_{gsr} \leq 3000\,km\,s^{-1}$, $|b| > 10^o$, $m_B \leq 18$ mag). Black dots highlight 1596 galaxies in the 2MASS XSC with K ≤ 10 mag that are contained within the same volume. A dashed line identifies the nominal 2MASS XSC limit at K = 14.5 mag.

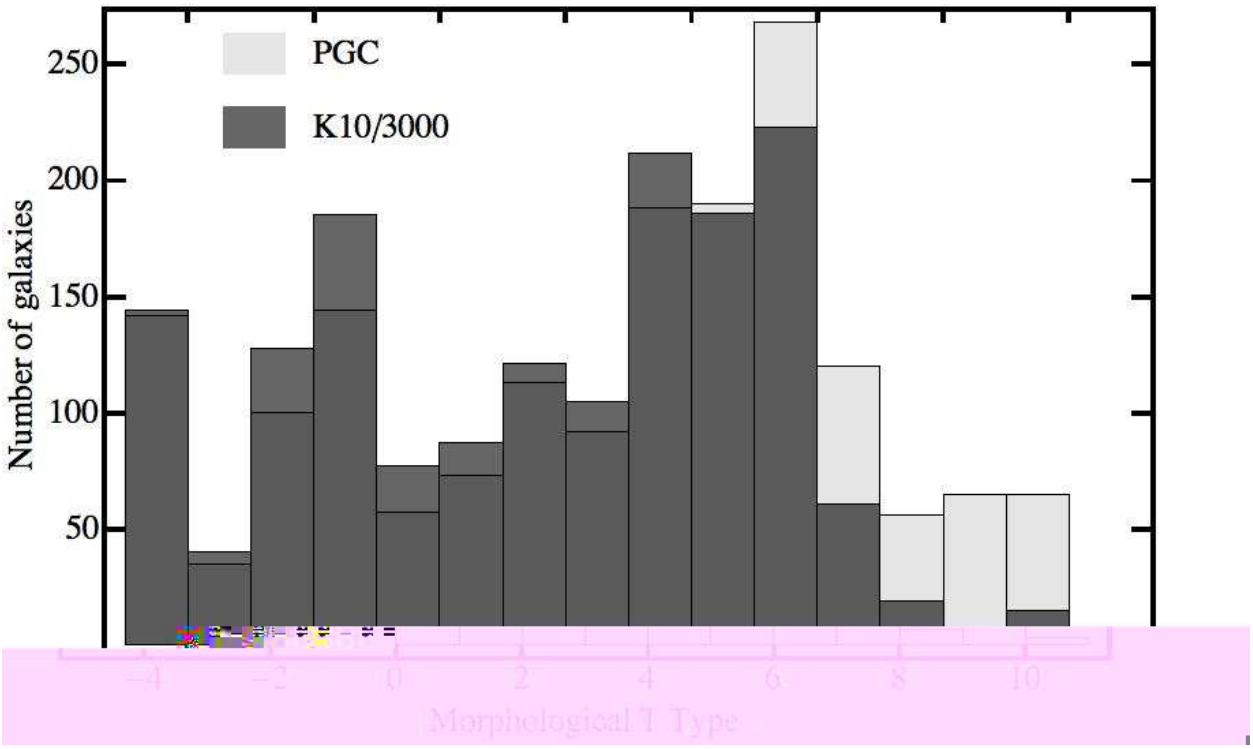

Fig. 3.— Histograms showing the distribution of morphological types for a B-band selected sample of 1711 nearby PGC galaxies ($V_{gsr} \leq 3000\,\mathrm{km\,s^{-1}}$, $|b| > 10^o$, $m_B \leq 13.5$ mag) versus the distribution of morphological types for 1610 galaxies in the K10/3000 sample, contained within the same volume.

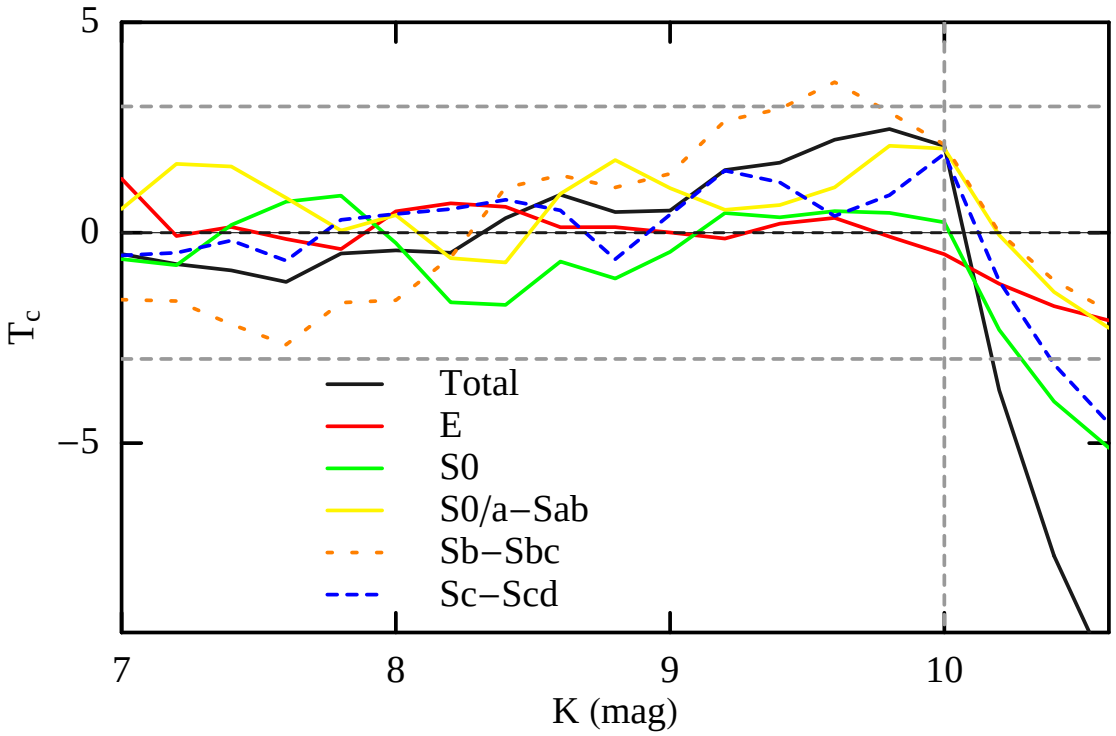

Fig. 4.— Rauzy test for 1601 galaxies in the K10/3000 sample. The test is applied to subsamples of the 2MASS XSC defined at progressively fainter apparent magnitudes. In the present figure these levels were defined at intervals of 0.1 magnitudes. The horizontal dashed lines show the levels from where the null hypothesis that the sample is complete can be rejected at 99.9% level, under the assumption of Gaussian statistics. The solid line indicates the expectation value of T_c. The vertical dashed line indicates the adopted limit of K=10. The colored lines indicate the results for the Rauzy test for different morphological subsamples indicated in the figure legend. The null hypothesis can be rejected with high confidence beyond $K \sim 10.1$ where the curve for T_c becomes systematically negative. Both the number counts and the Rauzy tests suggest that the current sample is not affected by incompleteness for the morphological types we are considering.

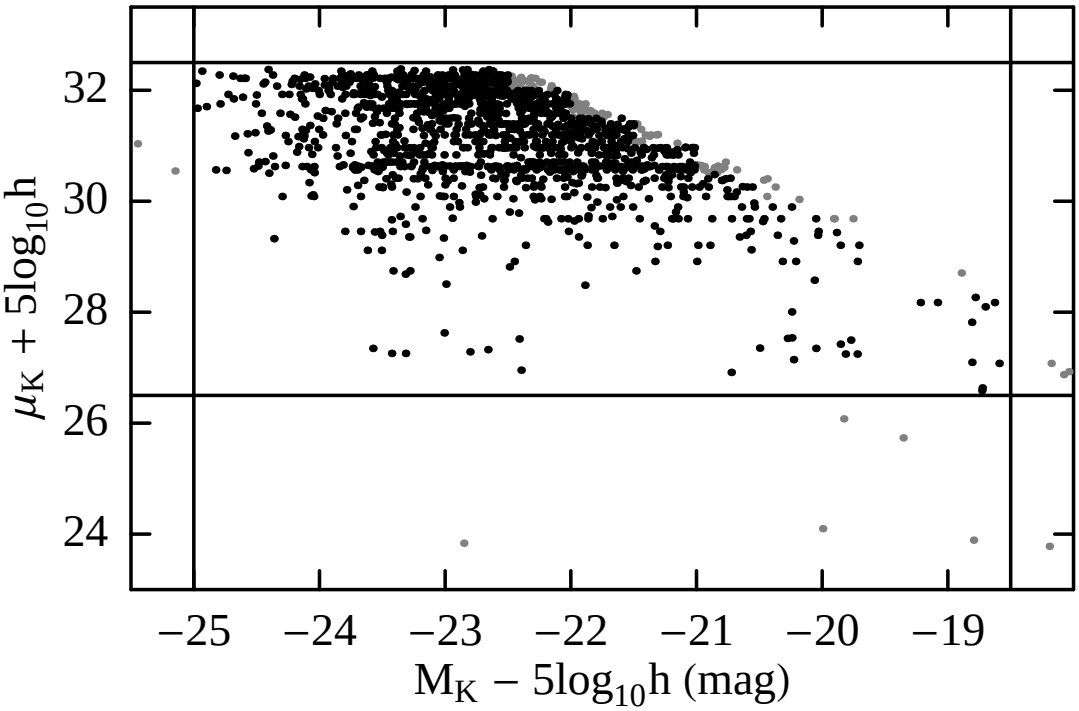

Fig. 5.— Absolute K magnitude, $M_K - 5\log_{10}h$, versus distance modulus, $\mu_K + 5\log_{10}h$, for 1349 galaxies (black dots). Gray dots identify 226 galaxies that are excluded by the binning process (see text for details). The vertical and horizontal lines identify the absolute magnitude and distance modulus limits imposed on the sample prior to computing the total LF (Table 2).

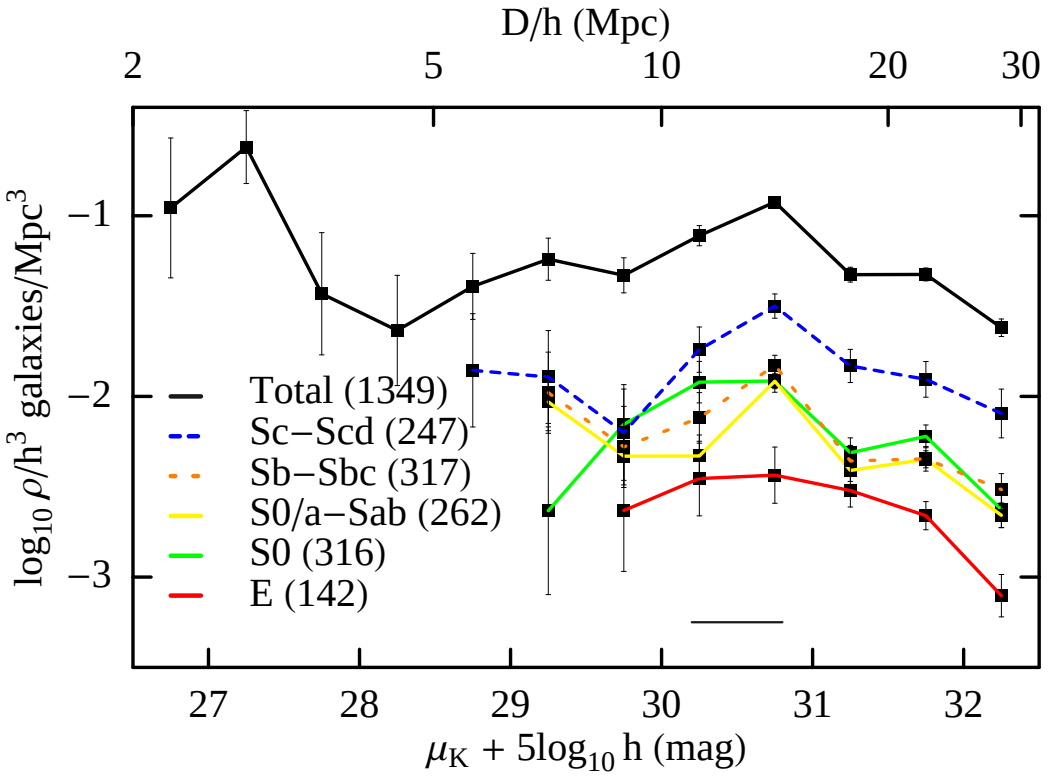

Fig. 6.— Number density as a function of distance modulus for 1349 galaxies in the K10/3000 sample segregated by morphological type. For reasons discussed in section 3 all plotted error bars are 50% larger than calculated using the maximum likelihood method outlined in the Appendix. The horizontal bar under the lowest curve identifies the extent of the Virgo cluster which constitutes only ∼14% of the total density in that distance range. Thus, one is cautioned against identifying density enhancements with individual structures because the density is angle averaged over essentially the whole sky.

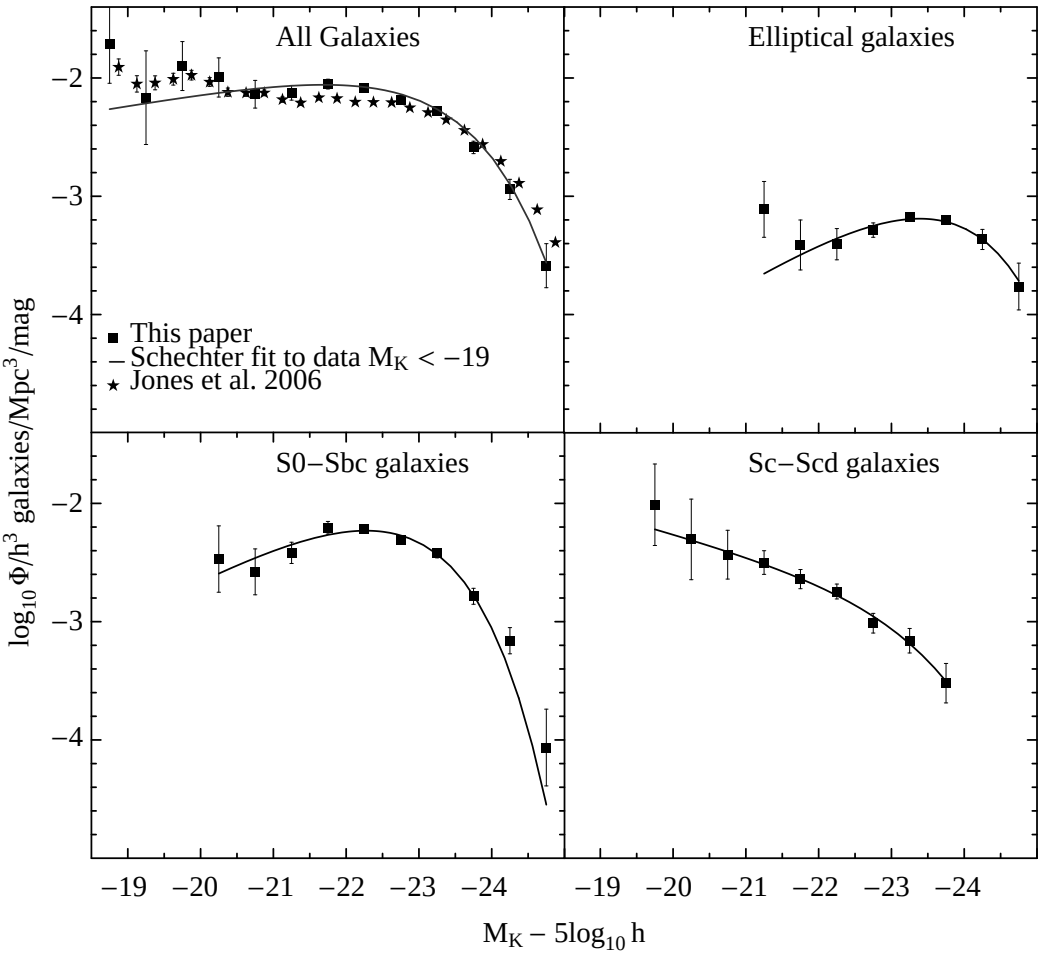

Fig. 7.— K-band isophotal luminosity functions for the K10/3000 sample. Filled squares represent the results of this paper and solid lines represent Schechter fits to the data (squares) *Top left panel:* Entire sample of 1349 galaxies. Increasing incompleteness is expected for $M_K - 5\log_{10}h \geq -19.75$ mag due to the omission of late-type (Sd and later) spiral and dwarf irregular (Im) galaxies. Stars identify the K-band SWML LF of Jones et al. (2006) for a different galaxy sample based on 2MASS isophotal magnitudes and a surface brightness dependent correction factor added to emulate total magnitudes. The Schecter fit excludes the first data point at $M_K - 5\log_{10}h = -18.75$. *Top right panel:* LF for 142 elliptical galaxies. The fit excludes the first data point at $M_K - 5\log_{10}h = -21.25$ which is attributed to the dwarf elliptical sequence. *Lower left panel:* Combined K-band isophotal LF for 904 lenticular (S0) and bulge-dominated spiral (S0/a - Sbc) galaxies. *Lower right panel:* LF for 247 late-type (Sc–Scd) spiral galaxies. The fit excludes the first data point at $M_K - 5\log_{10}h = -19.75$. For reasons discussed in section 3 all plotted error bars are 50% larger than calculated using the maximum likelihood method outlined in the Appendix.

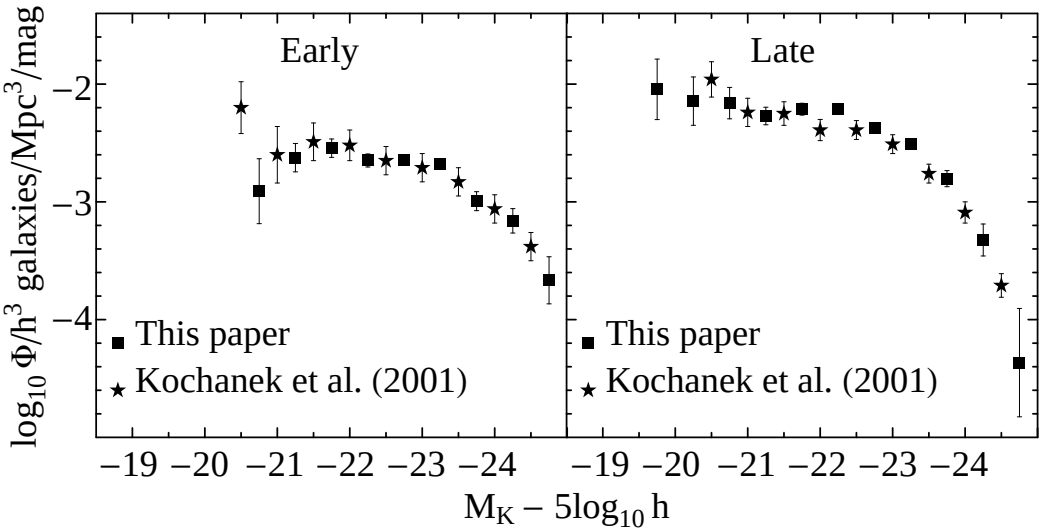

Fig. 8.— Comparison illustrating the agreement between our results and the cz > 2000 km/s, $K \leq 11.25$ mag, sample of Kochanek et al. (2001) when both are divided at T = −0.5 such that the early-type subsample includes elliptical and lenticular galaxies and the late-type subsample includes all galaxies classified S0/a and later. The Kochanek et al. (2001) LFs are based on 2MASS isophotal magnitudes. Plotted error bars on the squares are 50% larger than calculated using the maximum likelihood method outlined in the Appendix.

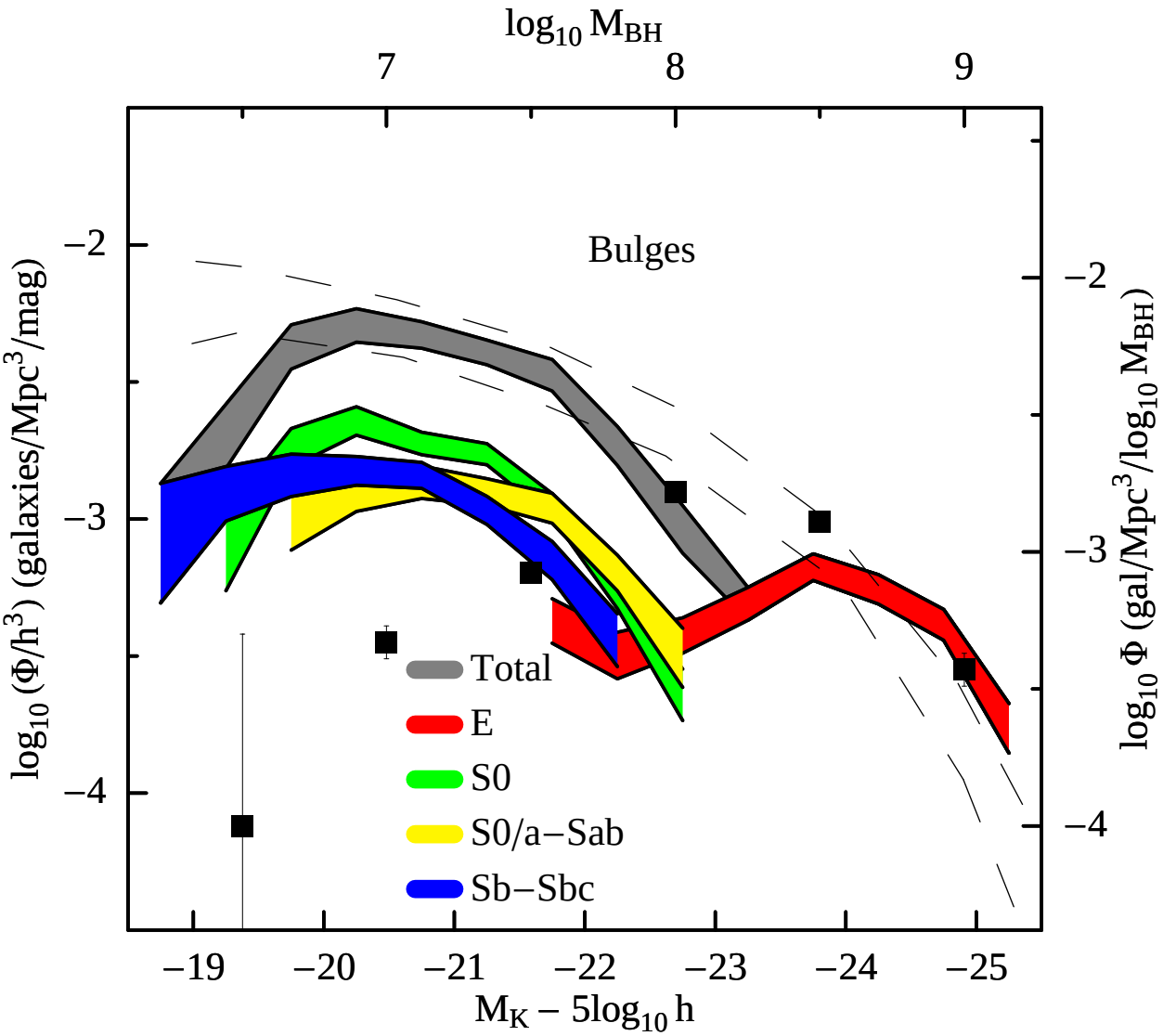

Fig. 9.— Bulge luminosity functions for galaxies in the K10/3000 sample segregated by morphology. The width of each band reflects the uncertainty associated with correcting total magnitudes to bulge magnitudes for the S0 - Sbc galaxies and correcting isophotal magnitudes to total magnitudes for the ellipticals. The total bulge LF merges with the elliptical LF near $M_K - 5\log_{10}h = -23.3$ mag. The upper abscissa and the right hand ordinate show the bulge LFs translated to black hole mass functions using the linear relation of Marconi & Hunt (2003); $\log_{10}(M_{BH}) = -3.757+1.13[(M_\odot-(M_K - 5\log_{10}h))/2.5]$ and $\log_{10}\phi(M_{BH}) = (2.5h^3/1.13)\log_{10}\phi(M)$. Black hole masses and mass functions are reported in solar units adopting $h = 0.7$ and $M_\odot = 3.32$ mag. Dashed lines show a range of BHMFs in the literature as summarized by Shankar, Weinberg & Miralda-Escudé (2009). Solid squares show the *All galaxies* black hole mass function from Graham et al. (2007).

Table 1. K10/3000 Galaxy Sample

PGC	NAME	2MASS ID	RA[a] Dec. Deg	DEC Dec. Deg.	K[b] mag	M_K[c] mag	B[d] mag	LGA[e]	Morphological[f] T type	Distance[g] Mpc	Quality[h] Distance
(1)	(2)	(3)	(4)	(5)	(6)	(7)	(8)	(9)	(10)	(11)	(12)
12651	NGC1316	03224178-3712295	50.67	-37.21	5.69	-25.97	9.44	Z	-1.7	21.48	q
41220	NGC4472	12294679+0800014	187.44	8.00	5.51	-25.66	9.27	Z	-4.8	17.14	q
30019	NGC3147	10165363+7324023	154.22	73.40	7.50	-25.47	11.26		3.9	39.26	
43296	NGC4696	12484927-4118399	192.21	-41.31	7.30	-25.45	11.65	Z	-3.7	35.48	q
13505	NGC1407	03401190-1834493	55.05	-18.58	6.86	-25.44	10.70	Z	-4.5	28.84	q
70090	IC1459	22571068-3627449	344.29	-36.46	6.93	-25.40	10.95	Z	-4.7	29.24	q

Note. — Table 1 is published in its entirety in the electronic edition of the *Astrophysical Journal*. A portion is shown here for guidance regarding its form and content. The galaxies are ordered by absolute K magnitude (column 7).

[a]J2000 coordinates taken from the 2MASS XSC based on the peak pixel (Jarrett et al. 2000).

[b]K magnitude measured within the 20 mag/arc sec^2 elliptical isophote, parameter `k_m_k20fe` in the 2MASS XSC. The photometric uncertainty in the magnitude is typically 3%.

[c]Absolute K magnitude computed using the distance in column 11 ($h = 0.75$).

[d]Total B magnitude taken from the Principal Galaxy Catalog (Paturel et al. 2003).

[e]Galaxy also listed in the Large Galaxy Atlas (Jarrett et al. 2003) based on the parameter `cc_flg = Z` in the 2MASS XSC.

[f]Morphological T type taken from the Principal Galaxy Catalog (Paturel et al. 2003).

[g]Distances provided by Tully (2007, private communication).

[h]"q" indicates quality distance (see text for details).

Table 2. K-band Luminosity Function Binning Parameters

Sample	$M_o - 5\log_{10}h$ mag	$M_A - 5\log_{10}h$ mag	$\mu_o + 5\log_{10}h$ mag	A mag	B	S
(1)	(2)	(3)	(4)	(5)	(6)	(7)
Total	−25	−18.5	26.5	13	12	17
Elliptical	−25	−21	29.5	8	6	11
S0	−24.5	−20.5	29	8	7	11
S0/a - Sab	−24.5	−21	29	7	7	11
Sb–Sbc	−24.5	−20.5	29	8	7	11
Sc–Scd	−24	−19.5	28.5	9	8	11

Note. — Following the notation of Choloniewski (1986), the apparent magnitude limit, $m_{lim} = 10$ mag, the bin size $\Delta = 0.5$ mag, the solid angle $\Omega = 3.3\pi$ steradians and the upper bound on the distance modulus, $\mu_B + 5\log_{10}h = 32.5$, for all samples

Table 3. K-band Luminosity Functions

Sample	$M_K - 5\log_{10}h$ mag	$\log_{10}\phi/h^3$ Gal Mpc^{-3} mag^{-1}	N Gal	Sample	$M_K - 5\log_{10}h$ mag	$\log_{10}\phi/h^3$ Gal Mpc^{-3} mag^{-1}	N Gal
(1)	(2)	(3)	(4)	(1)	(2)	(3)	(4)
Total	−24.75	−3.58 ± 0.12	12	Elliptical	−24.75	−3.76 ± 0.13	8
	−24.25	−2.94 ± 0.06	53	$T \leq -3.6$	−24.25	−3.36 ± 0.06*	20
	−23.75	−2.59 ± 0.04	120		−23.75	−3.20 ± 0.02*	29
	−23.25	−2.28 ± 0.02	242		−23.25	−3.17 ± 0.03*	31
	−22.75	−2.18 ± 0.02	303		−22.75	−3.28 ± 0.04*	24
	−22.25	−2.08 ± 0.02	273		−22.25	−3.40 ± 0.09	14
	−21.75	−2.05 ± 0.03	174		−21.75	−3.41 ± 0.14	8
	−21.25	−2.13 ± 0.04	97		−21.25	−3.11 ± 0.16	8
	−20.75	−2.14 ± 0.08	33				
	−20.25	−2.00 ± 0.11	18				
	−19.75	−1.90 ± 0.14	12				
	−19.25	−2.17 ± 0.26	3				
	−18.75	−1.70 ± 0.22	5				

Table 3—Continued

Sample	$M_K - 5\log_{10}h$ mag	$\log_{10}\phi/h^3$ Gal Mpc^{-3} mag^{-1}	N Gal	Sample	$M_K - 5\log_{10}h$ mag	$\log_{10}\phi/h^3$ Gal Mpc^{-3} mag^{-1}	N Gal
(1)	(2)	(3)	(4)	(1)	(2)	(3)	(4)
Lenticular	−24.25	−3.55 ± 0.11	13	Sa–Sab	−24.25	−4.06 ± 0.21	4
$-3.5 \leq T \leq -0.6$	−23.75	−3.41 ± 0.09	18	$-0.5 \leq T \leq 2.4$	−23.75	−3.26 ± 0.07	25
	−23.25	−2.84 ± 0.03*	66		−23.25	−2.97 ± 0.04*	49
	−22.75	−2.75 ± 0.02*	81		−22.75	−2.80 ± 0.02*	73
	−22.25	−2.73 ± 0.03*	64		−22.25	−2.76 ± 0.03*	57
	−21.75	−2.60 ± 0.05	48		−21.75	−2.69 ± 0.05	38
	−21.25	−2.76 ± 0.09	22		−21.25	−3.00 ± 0.11	13
	−20.75	−3.10 ± 0.22	4		−20.75	−3.08 ± 0.26	3
Sb–Sbc	−24.25	−3.43 ± 0.10	17	Sc–Scd	−23.75	−3.52 ± 0.11	14
$2.5 \leq T \leq 4.4$	−23.75	−3.14 ± 0.06	33	$4.5 \leq T \leq 6.5$	−23.25	−3.16 ± 0.07	32
	−23.25	−2.90 ± 0.04	58		−22.75	−3.01 ± 0.06	45
	−22.75	−2.79 ± 0.03*	74		−22.25	−2.74 ± 0.04*	55
	−22.25	−2.60 ± 0.02*	77		−21.75	−2.64 ± 0.05	42
	−21.75	−2.75 ± 0.06	34		−21.25	−2.50 ± 0.07	35
	−21.25	−2.90 ± 0.10	17		−20.75	−2.43 ± 0.14	12
	−20.75	−2.91 ± 0.20	5		−20.25	−2.30 ± 0.23	5
					−19.75	−2.01 ± 0.23	6

Note. — The sum of the number of galaxies within each Hubble type does not add up to the total number of galaxies because of the binning procedure inherent to the Choloniewski method and the fact that every plotted point is defined by a bin containing at least 3 objects. The uncertainties on the LF values are calculated using the maximum likelihood method outlined in the Appendix. Asterisks identify uncertainties that are less than $1/(2.3\sqrt{N})$ suggesting that the galaxy distribution is not Poisson but rather clumped in space and luminosity (section 3; Appendix). Galaxies are segregated according to morphological T types; a numerical system developed by de Vaucouleurs (1959) and de Vaucouleurs et al. (1991). The low luminosity end of the total LF, $M_K - 5\log_{10}h \geq -19.75$ mag, is defined by very late-types ($T \geq 6.5$) of which there are too few to define a LF separately.

Table 4. K-band Luminosity Function Fit Parameters

Sample	ϕ_*/h^3 galaxies Mpc^{-3} mag^{-1}	$\mathrm{M}_* - 5\log_{10}h$ mag	α
(1)	(2)	(3)	(4)
Total	$(11.5 \pm 3.4) \times 10^{-3}$	-23.41 ± 0.46	-0.94 ± 0.10
Elliptical	$(17.6 \pm 0.9) \times 10^{-4}$	-23.42 ± 0.17	-0.03 ± 0.16
S0 - Sbc	$(15.7 \pm 1.4) \times 10^{-3}$	-22.49 ± 0.20	-0.18 ± 0.16
Sc–Scd	$(15.9 \pm 4.8) \times 10^{-4}$	-23.33 ± 0.33	-1.41 ± 0.06

Note. — Columns (2) - (4) refer to Schechter function parameters (Figure 7). The uncertainties reflect unweighted fits to the data points.

Table 5. K-band Luminosity Density by Hubble Type

Sample (1)	$10^7 h \mathrm{L}_\odot\ \mathrm{Mpc}^{-3}$ (2)
Total	58 ± 12
Elliptical	8.1 ± 1.7
S0 - Sbc	34 ± 7
Sc–Scd	8.0 ± 1.6

Note. — The luminosity densties result from integration of the Schechter functions, defined in Table 4, between $-25 \leq \mathrm{M}_K \leq -19$.

Table 6. Bulge Luminosity Functions

Sample	$M_K - 5\log_{10}h$ mag	$\log_{10}\phi/h^3$ Gal Mpc^{-3} mag^{-1}	Sample	$M_K - 5\log_{10}h$ mag	$\log_{10}\phi/h^3$ Gal Mpc^{-3} mag^{-1}
(1)	(2)	(3)	(1)	(2)	(3)
Total	−25.25	−3.76 ± 0.09	Elliptical	−25.25	−3.76 ± 0.09
	−24.75	−3.38 ± 0.05	T≤−3.6	−24.75	−3.38 ± 0.06
	−24.25	−3.26 ± 0.05		−24.25	−3.25 ± 0.05
	−23.75	−3.17 ± 0.05		−23.75	−3.17 ± 0.05
	−23.25	−3.31 ± 0.06		−23.25	−3.31 ± 0.06
	−22.75	−3.03 ± 0.09		−22.75	−3.42 ± 0.06
	−22.25	−2.73 ± 0.07		−22.25	−3.50 ± 0.08
	−21.75	−2.47 ± 0.06		−21.75	−3.37 ± 0.08
	−21.25	−2.39 ± 0.04			
	−20.75	−2.33 ± 0.05			
	−20.25	−2.29 ± 0.06			
	−19.75	−2.37 ± 0.08			
	−19.25	−2.69 ± 0.11			
	−18.75	−3.09 ± 0.20			

Table 6—Continued

Sample	$M_K - 5\log_{10}h$ mag	$\log_{10}\phi/h^3$ Gal Mpc^{-3} mag^{-1}	Sample	$M_K - 5\log_{10}h$ mag	$\log_{10}\phi/h^3$ Gal Mpc^{-3} mag^{-1}
(1)	(2)	(3)	(1)	(2)	(3)
Lenticular	−22.75	−3.64 ± 0.09	Sa–Sab	−22.75	−3.50 ± 0.10
$-3.5 \leq T \leq -0.6$	−22.25	−3.27 ± 0.05	$-0.5 \leq T \leq 2.4$	−22.25	−3.20 ± 0.06
	−21.75	−2.95 ± 0.04		−21.75	−2.96 ± 0.05
	−21.25	−2.76 ± 0.04		−21.25	−2.90 ± 0.05
	−20.75	−2.72 ± 0.04		−20.75	−2.86 ± 0.06
	−20.25	−2.64 ± 0.05		−20.25	−2.88 ± 0.09
	−19.75	−2.74 ± 0.07		−19.75	−3.00 ± 0.10
	−19.25	−3.11 ± 0.14			
Sb - Sbc	−22.25	−3.44 ± 0.10			
$2.5 \leq T \leq 4.4$	−21.75	−3.15 ± 0.07			
	−21.25	−2.97 ± 0.05			
	−20.75	−2.84 ± 0.05			
	−20.25	−2.82 ± 0.05			
	−19.75	−2.84 ± 0.08			
	−19.25	−2.91 ± 0.10			
	−18.75	−3.09 ± 0.22			

Note. — The uncertainties reflect the ± 1σ range in the bulge/total luminosity ratio propagated through the LFs 55 times using a Monte-Carlo method (section 4.4).

Table 7. K-band Bulge Luminosity Density by Hubble Type

Sample (1)	$10^7 h \mathrm{L}_\odot\,\mathrm{Mpc}^{-3}$ (2)
Elliptical	10.7 ± 1.3
S0 - S0/a	2.6 ± 0.4
Sa - Sab	2.7 ± 0.6
Sb - Sbc	1.8 ± 0.3
Total	17.8 ± 1.5

Note. — The luminosity densities result from integration of the bulge LFs, shown in Figure 9, between $-25 \leq \mathrm{M}_K \leq -19$.